Laser-Driven Electron Acceleration in Infinite Vacuum

by

Liang Jie Wong

B.S. Electrical Engineering and Computer Science
University of California, Berkeley, 2008

Submitted to the Department of Electrical Engineering and Computer Science
in partial fulfillment of the requirements for the degree of

Master of Science in Electrical Engineering and Computer Science

at the

MASSACHUSETTS INSTITUTE OF TECHNOLOGY

June 2011

Author.....
Department of Electrical Engineering and Computer Science
May 20, 2011

Certified by .....
Franz X. Kärtner
Adjunct Professor of Electrical Engineering and Computer Science
Thesis Supervisor

Accepted by .....
Leslie A. Kolodziejski
Chairman, Department Committee on Graduate Students

Laser-Driven Electron Acceleration in Infinite Vacuum

by

Liang Jie Wong

B.S. Electrical Engineering and Computer Science

University of California, Berkeley, 2008

Submitted to the Department of Electrical Engineering and Computer Science
on May 20, 2011, in partial fulfillment of the
requirements for the degree of
Master of Science in Electrical Engineering and Computer Science

Abstract

I first review basic models for laser-plasma interaction that explain electron acceleration and beam confinement in plasma. Next, I discuss ponderomotive electron acceleration in infinite vacuum, showing that the transverse scattering angle of the accelerated electron may be kept small with a proper choice of parameters. I then analyze the direct (a.k.a. linear) acceleration of an electron in infinite vacuum by a pulsed radially-polarized laser beam, consequently demonstrating the possibility of accelerating an initially-relativistic electron in vacuum without the use of ponderomotive forces or any optical devices to terminate the laser field.

As the Lawson-Woodward theorem has sometimes been cited to discount the possibility of net energy transfer from a laser pulse to a relativistic particle via linear acceleration in unbounded vacuum, I derive an analytical expression (which I verify with numerical simulation results) defining the regime where the Lawson-Woodward theorem in fact allows for this. Finally, I propose a two-color laser-driven direct acceleration scheme in vacuum that can achieve electron acceleration exceeding 90% of the one-color theoretical energy gain limit, over twice of what is possible with a one-color pulsed beam of equal total energy and pulse duration.

Thesis Supervisor: Franz X. Kärtner
Title: Adjunct Professor of Electrical Engineering and Computer Science

Contents

1. Introduction **6**

2. Laser Wakefield Acceleration and Beam Guiding in Plasma **9**

2.1 Laser Wakefield Acceleration 10
2.2 Electron cavitation and self-focusing of short intense pulses in plasmas 17

3. Ponderomotive Acceleration of an Electron in Infinite Vacuum **31**

3.1 Electrodynamics of a single electron in a pulsed plane wave 31
3.2 Ponderomotive acceleration of an electron in infinite vacuum by a pulsed linearly-polarized Gaussian beam 35

4. Direct Acceleration of an Electron in Infinite Vacuum by a Radially-Polarized Beam **42**

4.1 Introduction 42
4.2 Theory of direct acceleration by a pulsed radially-polarized laser beam 43
4.3. Direct acceleration of an initially stationary electron 50
4.4. Direct acceleration of a pre-accelerated electron 56

5. Linear Acceleration of Relativistic Electrons In Infinite Vacuum Under the Lawson-Woodward Theorem **66**

6. Two-Color Laser-Driven Direct Acceleration of an Electron in Infinite Vacuum **74**

7. Conclusion **81**

Bibliography **83**

List of Figures

2.1.1 Plasma wave for low intensity driver beam....15
2.1.2 Plasma wave for high intensity driver beam....15
2.1.3 Field potential of plasma for high intensity driver beam....15
2.2.1 Electron cavitation....25
2.2.2 Value of $\rho_0\sqrt{\sigma}$ vs. power....26
2.2.3 Field pattern and electron density for fundamental plasma modes....28
2.2.4 Field pattern and electron density for second-order plasma modes....28
2.2.5 Field pattern and electron density for third-order plasma modes....29
2.2.6 Asymptotic behavior of $\rho_0\sqrt{\sigma}$ for higher-order plasma modes....29
3.1.1 Field and electron trajectory for an incident plane wave....34
3.2.1 Simulation schematic for ponderomotive electron acceleration....38
3.2.2 Electron energy and trajectory during ponderomotive acceleration....39
3.2.3 Final electron energy and scattering angle vs. CE phase for various waists....40
4.2.1 Simulation schematic for direct electron acceleration....46
4.3.1 Maximum energy gain and optimal beam waist vs. peak power....51
4.3.2 Maximum energy gain vs. initial electron position....51
4.3.3 Maxium energy gain and optimal initial position vs. peak power for various waists and pulse durations (electron initially at rest)....52
4.3.4 Close-up of maximum energy gain plot....55
4.4.1 Maximum energy gain and optimal protracted collision position vs. peak power for various waists and initial kinetic energies (7.5 fs pulse)....58
4.4.2 Maximum energy gain and optimal protracted collision position vs. peak power for various waists and initial kinetic energies (15 fs pulse)....59
4.4.3 Maximum energy gain and optimal protracted collision position vs. initial kinetic energy for various waists and peak powers (10 fs pulse)....60
4.4.4 Plot of maximum energy gain vs. protracted collision position to explain jumps in optimal protracted collision position as peak power increases....62
4.4.5 Kinetic energy variation with position of an intially-relativsitic electron accelerated by a pulsed radially-polarized laser beam....62
5.1 Fractional energy gain surface plots to illustrate accuracy of the analytical direct acceleration boundary expression....70
5.2 Fractional energy gain surface plot vs. peak power and beam waist....71
5.3 Fractional energy gain surface plot to illustrate relative independence of direct acceleration boundary from pulse duration....72
6.1 Sum-of-sinusoid plot to illustrate principle of two-color-laser-driven direct acceleration....75
6.2 Maxmimum gain and optimal parameter plots for two-color-laser-driven direct acceleration....77
6.3 Kinetic energy variation with position of an electron being accelerated by one-color and two-color pulses....79

6.4 Electric field profile at selected positions along the electron's trajectory.....80

1. Introduction

Electron acceleration is a rapidly-advancing field of scientific research that has widespread applications in industry and medicine [1,2]. With the invention of chirped pulse amplification [3], by which lasers with petawatt peak powers [4] and ultrahigh intensities [5] have been realized, there has been growing interest in laser-driven electron acceleration schemes due to their potential to offer compact and low-cost setups through high accelerator gradients that surpass those of conventional rf linear accelerators by several orders of magnitude [1,6,7].

The use of a plasma medium is one attractive way of achieving laser-driven electron acceleration [6]. Laser-driven plasma-based electron acceleration was demonstrated in the laboratory as early as 1995 (e.g.: [8]), but until 2004, accelerated bunches were characterized by an exponential energy distribution (and hence poor beam quality), with the most energetic electrons at the distribution's tail. In 2004, three groups ([9-11]) managed to produce electron bunches with an energy spread of a few percent and low divergence of several milliradians. This success in the electron acceleration mechanism called laser wakefield acceleration was attributed to the matching of the acceleration length to the dephasing length. Since then, many methods to obtain greater stability, reproducibility and higher electron energies in electron acceleration experiments have been proposed and demonstrated (see references in [6]). These include controlled injection of electrons with colliding laser pulses, the use of negative plasma density gradients and the use of plasma-channel-guided lasers.

A major challenge in laser-driven plasma-based electron acceleration is the existence of laser-plasma instabilities, which limit the laser propagation distance and degrades

accelerator performance [6]. The sources of these instabilities include stimulated forward and backward Raman scattering, self-modulation and parametric coupling to ion modes. The effort to circumvent these problems has led scientists to explore the alternative of laser-driven electron acceleration in vacuum.

Laser-driven electron acceleration in vacuum takes place primarily through either the ponderomotive force associated with the laser's transverse electric and magnetic field components (ponderomotive acceleration) [11-23], or the force exerted by the laser's longitudinal electric field component (direct acceleration) [24-32]. Direct acceleration of electrons in infinite vacuum by a radially-polarized laser is particularly attractive because such a scheme benefits from the low radiative losses of direct acceleration [31], the absence of limits on laser field intensity and electron confinement to the vicinity of the beam axis, which favors the production of mono-energetic and well-collimated electron beams [27, 32]. This scheme thus has major advantages that favor its application in the production of x-rays via inverse Compton Scattering [33].

In Chapter 2, I will review the theory of laser wakefield acceleration and self-focusing of the driver beam in the plasma. In Chapter 3, I will treat ponderomotive acceleration in infinite vacuum, examining first the case of an incident plane wave for analytical insight before simulating the more realistic case of a pulsed linearly-polarized Gaussian beam. In the course of this I will show that the transverse scattering angle of the accelerated electron may be kept small with a proper choice of parameters. In Chapter 4, I will analyze the direct acceleration of an electron in infinite vacuum by a pulsed radially-polarized laser beam, consequently demonstrating the possibility of accelerating an initially-relativistic electron in vacuum without the use of ponderomotive forces or any

optical devices to terminate the laser field. The Lawson-Woodward theorem has often been cited to discount such a possibility (e.g.: [15,23,24]). Therefore, in Chapter 5, I will reconcile the phenomenon of direct acceleration of a relativistic electron in infinite vacuum with the Lawson-Woodward theorem by showing how the space of laser and electron parameters contains a regime where the Lawson-Woodward theorem allows the electron to gain net energy. In Chapter 6, I will propose and analyze a direct electron acceleration scheme that uses a superposition of two pulsed radially-polarized laser beams an octave apart in carrier frequency. This two-color scheme exploits the Gouy phase shift to achieve electron acceleration exceeding 90% of the one-color theoretical energy gain limit, over twice of what is possible with a one-color pulsed beam of equal total energy and pulse duration.

2. Laser Wakefield Acceleration and Beam Guiding in Plasma

In this chapter, I study models of laser-plasma interaction to understand the electron-acceleration and beam confinement properties of plasma. Although the subject of this thesis is laser-driven electron acceleration in vacuum, one is motivated by the experimental successes of plasma-based electron acceleration [9-11] to obtain intuition about laser-driven electron acceleration by understanding the factors that enable it in plasma-based schemes.

In laser wakefield acceleration (LWFA), a short (sub-picosecond) high-intensity pulse moves through a plasma with a certain ambient electron density. Interactions between the laser pulse and the electrons causes the electron density to vary from its ambient value. The moving electrons and changing charge distribution may give rise to large amplitude longitudinal electric field oscillations that can persist in the plasma even after the laser pulse has traveled on. The short, high-intensity laser pulse thus drives a plasma wave in its wake, which may be used to accelerate electrons in the plasma or injected particles to very high energies.

There are, however, several challenges associated with LWFA. One of them is the need to create a guiding channel for the laser beam to overcome beam diffraction. One method is by using preformed plasma-density channels (e.g. [34]). However, it turns out that at laser powers above a certain critical value, it may be possible to guide the laser pulse over several Rayleigh lengths without the use of a density channel due to a combination of relativistic self-focusing and ponderomotive self-channeling. This is what happens in the "blow-out" (or "bubble") regime [35], a regime in which the recent experimental successes [9-11] have been realized. In this regime, the radial

ponderomotive force of a laser pulse propagating in an initially uniform plasma expels electrons from the axis, creating a density channel. When the laser intensity is high enough, a complete absence of electrons, called an electron cavity, develops around the axis [36,37]. This can enhance the effects of relativistic self-focusing, which is critical to the guiding of the laser pulse and hence to electron acceleration.

In Section 2.1, I introduce the physics of LWFA, following the steps of [38]. In Section 2.2, I will derive the theory of electron cavitation and self-focusing in a plasma with a ultrashort, high-intensity pulse traveling through it, following the steps of [36]. In addition, I will show that the theory of [36] also predicts the existence of higher-order plasma modes, an observation which was not made in [36]. Higher order modes have been found useful in increasing the matched electron beam radius in wakefield acceleration, leading to increased charge and efficiency while maintaining low bunch emittance [39].

2.1 Laser Wakefield Acceleration

Maxwell's equations, expressed in terms of the retarded potentials in the Coulomb gauge, together with the Newton-Lorentz equation give the following set of coupled equations in a cold plasma (where collisions and thermal effects are ignored):

$$\nabla^2 \vec{A} - \frac{1}{c^2}\frac{\partial^2 \vec{A}}{\partial t^2} = \frac{1}{c^2}\frac{\partial}{\partial t}\nabla\phi - \mu_0 \vec{J}\,, \tag{2.1.1a}$$

$$\nabla^2 \phi = -\frac{\rho}{\varepsilon_0}, \tag{2.1.1b}$$

$$\frac{d\vec{p}}{dt} = -e\left(-\frac{\partial \vec{A}}{\partial t} - \nabla\phi + \vec{v}\times\left(\nabla\times\vec{A}\right)\right), \tag{2.1.1c}$$

$$\frac{\partial n}{\partial t}+\nabla\cdot\left(n\vec{v}\right)=0, \tag{2.1.1d}$$

where $\vec{A}$ and ϕ are the field potentials corresponding to the Coulomb gauge condition $\nabla\cdot\vec{A}=0$, $\rho=-e\left(n-n_a\right)$, e is the absolute value of an electron's charge, n the electron density, n_a the ambient electron density, $\vec{J}=-en\vec{v}$ the current density, $\vec{v}$ the electron velocity, $\vec{p}=\gamma m\vec{v}$ the electron momentum, $\gamma=\left(1-\vec{v}^2/c^2\right)^{-1/2}=\left(1+\vec{p}^2/m^2c^2\right)^{1/2}$ the Lorentz factor, m the electron rest mass, c the speed of light in vacuum. The plasma frequency is $\omega_p\equiv\sqrt{ne^2/m\varepsilon_0}$. The Coulomb gauge has been used because it very conveniently allows us to associate the plasma wakefield with ϕ and the driving laser pulse with $\vec{A}$.

Applying the normalizations $\vec{a}\equiv e\vec{A}/mc$, $\varphi\equiv e\phi/mc^2$, $\tilde{n}\equiv n/n_a$, $T\equiv ct$ and using $k_p\equiv\omega_p/c$, we transform equations (2.1.1a-d) to

$$\nabla^2\vec{a}-\frac{\partial^2\vec{a}}{\partial T^2}=\frac{\partial}{\partial T}\nabla\varphi+k_p^2\tilde{n}\vec{\beta}, \tag{2.1.2a}$$

$$\nabla^2\varphi=k_p^2\left(\tilde{n}-1\right), \tag{2.1.2b}$$

$$\frac{d\left(\gamma\vec{\beta}-\vec{a}\right)}{dT}=\nabla\varphi-\hat{x}\left(\vec{\beta}\cdot\frac{\partial\vec{a}}{\partial x}\right)-\hat{y}\left(\vec{\beta}\cdot\frac{\partial\vec{a}}{\partial y}\right)-\hat{z}\left(\vec{\beta}\cdot\frac{\partial\vec{a}}{\partial z}\right), \tag{2.1.2c}$$

$$\frac{\partial\tilde{n}}{\partial T}+\nabla\cdot\left(\tilde{n}\vec{\beta}\right)=0, \tag{2.1.2d}$$

where we have rearranged (2.1.1c) using the identity $\vec{v}\times\left(\nabla\times\vec{A}\right)=\nabla_A\left(\vec{v}\cdot\vec{A}\right)-\left(\vec{v}\cdot\nabla\right)\vec{A}$. If we consider only variations in z and T, assuming transversal spatial variations to be 0 for all variables, we can simplify (2.1.2a-d) to give

$$\frac{\partial^2 \vec{a}}{\partial z^2} - \frac{\partial^2 \vec{a}}{\partial T^2} = \frac{\partial}{\partial T}\nabla\varphi + k_p^2 \tilde{n}\vec{\beta}, \tag{2.1.3a}$$

$$\frac{\partial^2 \varphi}{\partial z^2} = k_p^2(\tilde{n} - 1), \tag{2.1.3b}$$

$$\frac{d(\gamma\vec{\beta} - \vec{a})}{dT} = \hat{z}\frac{\partial \varphi}{\partial z} - \hat{z}\left(\vec{\beta}\cdot\frac{\partial \vec{a}}{\partial z}\right), \tag{2.1.3c}$$

$$\frac{\partial \tilde{n}}{\partial T} + \nabla\cdot(\tilde{n}\vec{\beta}) = 0, \tag{2.1.3d}$$

Equating transverse components of (2.1.3c) gives us (allowing subscript t to denote transversal components and subscript 0 to denote initial time) $\gamma\beta_t - a_t = \gamma_0\beta_{t0} - a_{t0}$. If we assume the plasma is stationary and the field is absent at initial time, we have

$$\gamma\beta_t = a_t \tag{2.1.4}$$

We also assume that $\vec{a}$ has no longitudinal component. Equating the longitudinal components of (2.1.3c) gives

$$\frac{d(\gamma\beta_z)}{dT} = \frac{\partial \varphi}{\partial z} - \beta_t\frac{\partial a_t}{\partial z} = \frac{\partial \varphi}{\partial z} - \frac{1}{2\gamma}\frac{\partial a_t^2}{\partial z}, \tag{2.1.5}$$

where we have applied (2.1.4) in the rightmost equality. Note that the first and second terms in the rightmost expression correspond to acceleration by the plasma wakefield and by the ponderomotive force, which results directly from the transverse electromagnetic field components of the laser itself, respectively. Next, we likewise equate the transverse and longitudinal components of (2.1.3a) separately. The longitudinal part gives us a redundant equation. The transverse part gives

$$\frac{\partial^2 a_t}{\partial z^2} - \frac{\partial^2 a_t}{\partial T^2} = k_p^2 \tilde{n}\beta_t, \tag{2.1.6}$$

Equations (2.1.4), (2.1.5) and (2.1.6) may be used to replace (2.1.3c) and (2.1.3a).

Now we transform the basis of our coordinates, defining $\xi \equiv z - T$, from (z,T) to (ξ,T), we find that our set of coupled differential equations may be written in the form

$$2\frac{\partial^2 a_t}{\partial\zeta\partial T} - \frac{\partial^2 a_t}{\partial T^2} = k_p^2 \tilde{n}\frac{a_t}{\gamma} \tag{2.1.7a}$$

$$\frac{\partial^2 \varphi}{\partial \xi^2} = k_p^2(\tilde{n} - 1) \tag{2.1.7b}$$

$$\frac{\partial}{\partial\xi}(\gamma(1-\beta_z) - \varphi) = -\frac{\partial}{\partial T}(\gamma\beta_z) \tag{2.1.7c}$$

$$\frac{\partial}{\partial\xi}(\tilde{n}(1-\beta_z)) = \frac{\partial\tilde{n}}{\partial T} \tag{2.1.7d}$$

The reason for our change of reference frame is so that we may make a distinction between variations in T and variations in ξ. We assume variations in T to be much smaller than all other variations in what is called the quasi-static approximation. Applying the quasi-static approximation, then, we set the right-hand-sides of (2.1.7c) and (2.1.7d) to 0 and obtain

$$\gamma(1-\beta_z) - \varphi = 1 \tag{2.1.8}$$

$$\tilde{n}(1-\beta_z) = 1 \tag{2.1.9}$$

where $\tilde{n}_0 = 1$, $\beta_0 = 0$, $\varphi_0 = 0$ at first (i.e.: the plasma is initially stationary and uniformly at its ambient density, and there is, of course, no wakefield). Noting that we can also write $\gamma = \sqrt{(1+a_t^2)/(1-\beta_z^2)}$, we use (2.1.8) and (2.1.9) in (2.1.7b) to obtain

$$\frac{d^2\varphi}{d\xi^2} = \frac{k_p^2}{2}\left(\frac{1+a_t^2}{(1+\varphi)^2} - 1\right) \tag{2.1.10}$$

(2.1.10) may be solved numerically given $a_t(\xi)$. The remaining unknowns may then be computed as

$$\tilde{n} = 1 + \frac{1}{2}\left(\frac{1+a_t^2}{(1+\varphi)^2} - 1\right) \tag{2.1.11}$$

$$\gamma = \frac{1+a_t^2+(1+\varphi)^2}{2(1+\varphi)} \tag{2.1.12}$$

$$\beta_z = \frac{1+a_t^2-(1+\varphi)^2}{1+a_t^2+(1+\varphi)^2} \tag{2.1.13}$$

Note that we have not yet made use of (2.1.7a). (2.1.7a), which describes the evolution of a_t, is important in determining a pulse envelope that preserves the validity of the quasistatic approximation. Suppose that the beam envelope of a_t (without the pulse but including the carrier) varies at a rate of $1/T_e$ in T and of $k = \omega/c$ in ξ. For the quasistatic approximation to hold, the variation in T of a_t must be small compared to its variation in ξ. Ignoring the pulse envelope, we see that (2.1.7a) becomes

$$\frac{2k}{T_e} + \frac{1}{T_e^2} \approx \frac{2k}{T_e} = \frac{k_p^2\tilde{n}}{\gamma} \Rightarrow T_e = \frac{2\gamma k}{k_p^2\tilde{n}} \tag{2.1.14}$$

where we used the fact that $2k >> 1/T_e$. Hence, we are justified in using the quasistatic approximation as long as we choose the pulse duration T_L to be such that $T_L << T_e$. The narrow pulse envelope ensures that the variation in T of the beam envelope seen within the pulse envelope will always be negligible.

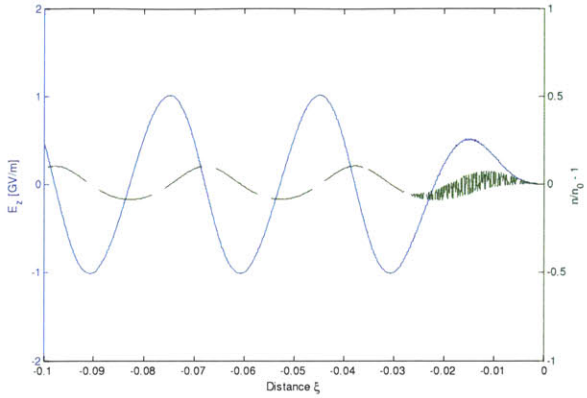

Fig.2.1.1: Density variation and longitudinal electric field component for $a_{L0} = 0.5$. Notice that the period of oscillation for this slightly nonlinear case is close to plasma period $\lambda_p = L = 0.03\text{cm}$.

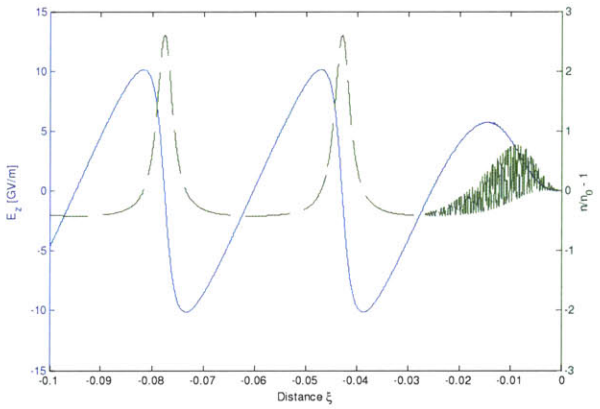

Fig.2.1.2: Density variation and longitudinal electric field component for $a_{L0} = 2$. Notice that the period of oscillation for this highly nonlinear case is almost 0.04cm, significantly greater than plasma period $\lambda_p = L = 0.03\text{cm}$.

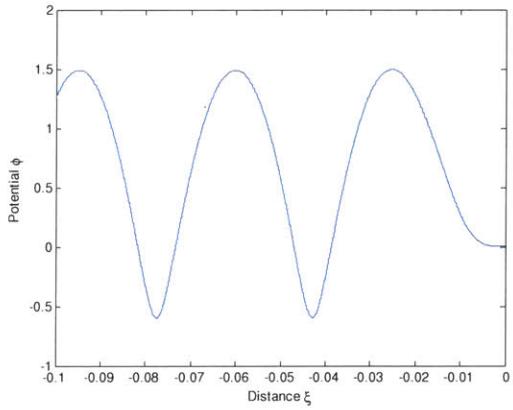

Fig.2.1.3: Field potential φ for $a_{L0} = 2$. Notice that even where n/n_a fluctuates rapidly, φ is predominantly slowly varying within the laser pulse.

To illustrate the effect on the plasma of an incident laser pulse under the quasistatic approximation, let us use a pulse of a form

$$a_t = \begin{cases} a_{L0} \sin\left(\frac{\pi\xi}{L}\right)\cos\left(\frac{2\pi}{\lambda}\xi\right) & -L \le \xi \le 0 \\ 0 & \text{otherwise} \end{cases} \tag{2.1.15}$$

Figures 2.1.1 and 2.1.2 show the plasma density variation $n/n_a - 1$ and the longitudinal electric field $E_z = -\partial\phi/\partial z$ for a laser pulse envelope given by (2.1.15). $L = \lambda_p = 0.03\text{cm}$, $\lambda = 10\mu\text{m}$, $a_{L0} = 0.5$ in Fig. 2.1.1, corresponding to a slightly nonlinear case, whereas $a_{L0} = 2$ in Fig. 2.1.2, corresponding to a highly nonlinear case. The term "nonlinear" used here refers to the behavior of differential equation (2.1.10), which, though apparently nonlinear, approximates a linear differential equation for small a_{L0}. To see this, note that for small a_t and φ (2.1.10) becomes

$$\begin{aligned} \frac{d^2\varphi}{d\xi^2} &\approx \frac{k_p^2}{2}\left(\left(1+a_t^2\right)(1-2\varphi)-1\right) \\ &\approx \frac{k_p^2}{2}\left(a_t^2 - 2\varphi\right) \\ &\approx -k_p^2\varphi \end{aligned} \tag{2.1.16}$$

Note that the equation is already a linear (inhomogeneous) differential equation in the second line of (2.1.16). In the third line we let $a_t = 0$ to look at the wakefield region $\xi < -L$ that the pulse has already passed over. Clearly, the solutions to the third line of (2.1.16) are sinusoids of period λ_p. Therefore, we expect φ to oscillate sinusoidally in the wake of the pulse with a period of about λ_p when a_t and φ are small.

The steepening of the longitudinal electric wakefield and the increase in the period of the field and charge density variation behind the pulse as a_{L0} increases is evident from Figs. 2.1.1 and 2.1.2. The period of oscillation increases from approximately $\lambda_p = 0.03\text{cm}$ (which the analytical approximations in (2.1.16) predicts) for $a_{L0} = 0.5$ in Fig. 2.3.1 to almost 0.04cm for $a_{L0} = 2$ in Fig. 2.1.2. The density oscillations also become highly peaked. Fig. 2.1.3 shows that the field potential φ corresponding to the plasma charge separation is mainly slowly varying within the laser pulse even though the charge density varies rapidly (Fig. 2.1.2). The figure also shows that φ can be negative behind the laser pulse. As mentioned before, Laser Wakefield Acceleration exploits the large amplitude longitudinal electric field associated with the plasma waves in the laser pulse's wake to accelerate an injected beam of electrons to high energies. Further work in [41] has shown that the energy gain of a trapped electron scales as $2\gamma_p^2 E_z^2$ in the large wave amplitude limit, where γ_p is the Lorentz factor associated with the plasma wave phase velocity and E_z is the electric field amplitude of the nonlinear plasma wave.

2.2 Electron cavitation and self-focusing of short intense pulses in plasmas

As in the previous section, we begin with an intense laser beam in a cold plasma where ions are assumed to be fixed and uniformly distributed. The equations that govern the interaction between the laser's electromagnetic field and the plasma's electrons are:

$$\nabla^2 \vec{A} - \frac{1}{c^2}\frac{\partial^2 \vec{A}}{\partial t^2} = -\mu_0 \vec{J}\,, \tag{2.2.1a}$$

$$\nabla^2 \phi - \frac{1}{c^2}\frac{\partial^2 \phi}{\partial t^2} = -\frac{\rho}{\varepsilon_0}, \tag{2.2.1b}$$

$$\nabla \cdot \vec{A} + \frac{1}{c^2}\frac{\partial \phi}{\partial t} = 0, \tag{2.2.1c}$$

$$\frac{d\vec{p}}{dt} = -e\left(-\frac{\partial \vec{A}}{\partial t} - \nabla\phi + \vec{v} \times \left(\nabla \times \vec{A}\right)\right), \tag{2.2.1d}$$

$$\frac{\partial n}{\partial t} + \nabla \cdot \left(n\vec{v}\right) = 0, \tag{2.2.1e}$$

where all variables are as defined before. (2.2.1) are the same set of equations as (2.1.1) except that here we employ the Lorentz gauge instead, after the fashion of [36]. For convenience, we introduce normalizations and make substitutions such that $\vec{p}/mc \to \vec{p}$, $e\vec{A}/mc \to \vec{A}$, $e\phi/mc^2 \to \phi$, $\omega t \to t$ (ω being the angular frequency of the laser), $\omega\vec{r}/c \to \vec{r}$ ($\vec{r}$ being the position vector) and $n/n_a \to n$. This gives us:

$$\nabla^2 \vec{A} - \frac{\partial^2 \vec{A}}{\partial t^2} = \varepsilon^2 n\vec{v}, \tag{2.2.2a}$$

$$\nabla^2 \phi - \frac{\partial^2 \phi}{\partial t^2} = \varepsilon^2 (n-1), \tag{2.2.2b}$$

$$\nabla \cdot \vec{A} + \frac{\partial \phi}{\partial t} = 0, \tag{2.2.2c}$$

$$\frac{d\left(\vec{p} - \vec{A}\right)}{dt} = \nabla\phi - \hat{x}\left(\vec{v} \cdot \frac{\partial \vec{A}}{\partial x}\right) - \hat{y}\left(\vec{v} \cdot \frac{\partial \vec{A}}{\partial y}\right) - \hat{z}\left(\vec{v} \cdot \frac{\partial \vec{A}}{\partial z}\right), \tag{2.2.2d}$$

$$\frac{\partial n}{\partial t} + \nabla \cdot \left(n\vec{v}\right) = 0, \tag{2.2.2e}$$

where $\vec{v} = \vec{p}/\gamma$, $\gamma = \sqrt{1 + |\vec{p}|^2}$, $\varepsilon = \omega_p/\omega$, $\omega_p = \sqrt{n_a e^2/\varepsilon_0 m}$ is the natural plasma frequency.

We assume an underdense plasma, for which $\varepsilon << 1$, and that our laser beam satisfies the slowly varying envelope approximation. This allows us to use the multiple scale

method and expand all physical quantities as $G(\vec{r},t)=G_0(\xi,x_1,y_1,z_2)+\varepsilon G_1(\xi,x_1,y_1,z_2)$, where $\xi=z-\alpha t$, $(x_1,y_1)=\varepsilon(x,y)$, $z_2=\varepsilon^2 z$ and $\alpha\equiv\omega/kc=v_{ph}/c$ is the normalized phase velocity in the z direction v_{ph} of any function of ξ. We assume that this phase velocity is approximately c so that $(\alpha-1)\sim\varepsilon^2$, which implies $\alpha_1^{\,2}\equiv(\alpha^2-1)/\varepsilon^2\sim 1$.

The multiple scale analysis assumes that for each physical quantity, the variation in ξ is larger by a factor of ε^{-1} than the variation in (x,y), and larger by a factor of ε^{-2} than the variation in z. In other words, for each physical quantity, variations in ξ, x_1, y_1 and z_2, are of the same order of magnitude. All physical quantities may also contain a perturbation (i.e. G_1) that is smaller than the lowest order part (i.e. G_0) by a factor of approximately ε^{-1} (and so G_0 and G_1 are of the same order of magnitude).

We let $\partial/\partial z\to\partial/\partial z+\partial/\partial\xi$, $\partial/\partial t\to-\alpha\partial/\partial\xi$, $\partial^2/\partial t^2\to\alpha^2\partial^2/\partial\xi^2$, $\partial^2/\partial z^2\to\partial^2/\partial z^2+2\partial^2/\partial\xi\partial z+\partial^2/\partial\xi^2$ and $\nabla^2\to\nabla_t^{\,2}+\partial^2/\partial z^2+2\partial^2/\partial\xi\partial z+\partial^2/\partial\xi^2$, where $\nabla_t^{\,2}$ is the transverse Laplacian, in equations (2.2.2). This gives us, considering just the lowest order terms:

$$\left[\nabla_{t1}^2+2\frac{\partial^2}{\partial\xi\partial z_2}-\alpha_1^{\,2}\frac{\partial^2}{\partial\xi^2}\right]\vec{A}_0=n_0\vec{v}_0, \tag{2.2.3a}$$

$$\left[\nabla_{t1}^2+2\frac{\partial^2}{\partial\xi\partial z_2}-\alpha_1^{\,2}\frac{\partial^2}{\partial\xi^2}\right]\phi_0=n_0-1, \tag{2.2.3b}$$

$$\frac{\partial(A_{0z}-\alpha\phi_0)}{\partial\xi}=0, \tag{2.2.3c}$$

$$(v_{0z}-\alpha)\frac{\partial}{\partial\xi}(\vec{p}_0-\vec{A}_0)=\hat{z}\left(\frac{\partial\phi_0}{\partial\xi}-\frac{\partial\vec{A}_0}{\partial\xi}\cdot\vec{v}_0\right), \tag{2.2.3d}$$

$$\frac{\partial n_0(v_{0z}-\alpha)}{\partial \xi}=0. \qquad (2.2.3e)$$

To proceed, we use the ansatz $\vec{A}_0(\vec{r},t)=0.5\left[(\hat{x}+i\hat{y})A_0(\rho,z)e^{i\xi\alpha}+c.c.\right]$ for a circularly-polarized laser beam with an axisymmetric amplitude A_0, ρ being the radial coordinate of the cylindrical coordinate system. Note that $\left|\vec{A}_0\right|^2=\left|A_0\right|^2$ does not contain $e^{\pm i2\xi\alpha}$ terms by virtue of the fact that $\vec{A}_0$ is circularly polarized. Also, $e^{i\xi\alpha}$ is simply $e^{i(kz-\omega t)}$ in un-normalized variables. From (2.2.3c) and (2.2.3d) we see that (using subscript t to indicate transverse component)

$$\frac{\partial}{\partial \xi}\left(\vec{p}_{0t}-\vec{A}_0\right)=\frac{\partial \phi_0}{\partial \xi}=0.$$

Furthermore, equations (2.2.3) allow us to self-consistently set

$$\frac{\partial p_{0z}}{\partial \xi}=\frac{\partial v_{0z}}{\partial \xi}=\frac{\partial n_0}{\partial \xi}=p_{0z}=v_{0z}=0,$$

$$\vec{p}_0=\vec{A}_0. \qquad (2.2.4)$$

Physically, (2.2.4) means that the plasma electrons move circularly about the axis in planes transverse to the axis. Equating the terms of the next highest order in (2.2.2d), bearing (2.2.4) in mind, gives us

$$(v_{0z}-\alpha)\frac{\partial}{\partial \xi}\left(\vec{p}_1-\vec{A}_1\right)=\hat{z}\left(\frac{\partial \phi_1}{\partial \xi}-\frac{\partial \vec{A}_1}{\partial \xi}\cdot\vec{v}_0-\frac{\partial \vec{A}_0}{\partial \xi}\cdot\vec{v}_1\right)+\nabla_t\phi_0-\hat{x}\vec{v}_0\cdot\frac{\partial \vec{A}_0}{\partial x_1}-\hat{y}\vec{v}_0\cdot\frac{\partial \vec{A}_0}{\partial y_1},$$

which becomes, upon self-consistently setting $\partial\left(\vec{p}_1-\vec{A}_1\right)/\partial\xi=0$, noting that to first order the Lorentz factor $\gamma_0=\sqrt{1+\left|\vec{A}_0\right|^2}=\sqrt{1+\left|A_0\right|^2}$ and $\vec{v}_0=\vec{p}_0/\gamma_0=\vec{A}_0/\gamma_0$, and equating transverse components on both sides of the equation,

$$\nabla_t \phi_0 = \nabla_t \gamma_0 , \tag{2.2.5}$$

which represents the balance between the electrostatic and ponderomotive forces on the electrons. We substitute (2.2.5) and previous relations into (2.2.3a) and (2.2.3b) to obtain

$$\left[\nabla_{t1}^2 + 2\frac{\partial^2}{\partial\xi\partial z_2} - \alpha_1^{\,2}\frac{\partial^2}{\partial\xi^2}\right]\vec{A}_0 = n_0\frac{\vec{A}_0}{\gamma_0}, \tag{2.2.6}$$

$$n_0 = 1 + \nabla_{t1}^2\gamma_0 . \tag{2.2.7}$$

Since the operators acting on $\vec{A}_0$ on either side of (2.2.6) are real, $\vec{A}_0$ may be replaced by any complex expression the real part of which gives the actual (real-valued) $\vec{A}_0$. We may thus set $\vec{A}_0 = (\hat{x} + i\hat{y})A_0 e^{i\xi/\alpha}$ in (2.2.6), bearing in mind that the actual value for the field quantity is proportional to $\mathrm{Re}\{\vec{A}_0\}$, so that (2.2.6) becomes

$$\left[\nabla_{t1}^2 + \frac{2i}{\alpha}\frac{\partial}{\partial z_2} + \sigma\right]A_0 = n_0\frac{A_0}{\gamma_0}, \tag{2.2.8}$$

where $\sigma \equiv (\alpha^2 - 1)/\varepsilon^2\alpha^2$.

Equation (2.2.7) is valid only for non-negative values of n_0, because a negative electron density is physically unrealistic. To make (2.2.7) valid for all situations we set $n_0 = 0$ whenever n_0 falls below zero. To find the field and electron distribution in a plasma, we thus solve the two equations

$$\left[\nabla_t^2 + 2i\frac{\partial}{\partial z} + \sigma\right]A = n\frac{A}{\gamma}, \tag{2.2.9}$$

$$n = \theta(1 + \nabla_t^2\gamma), \tag{2.2.10}$$

where for convenience we have dropped the subscripts. (2.2.9) is simply (2.2.8) with α set to its lowest order value of 1 and θ is the ramp function such that $\theta(x) = x, x \geq 0$;

$\theta(x)=0, x<0$. As we will see later, large ponderomotive forces that arise when the laser intensity is high enough may push all the electrons out of some region, leading to a complete absence of electrons in a phenomenon that has been dubbed "electron cavitation" [36].

To find the stationary states of (2.2.9) and (2.2.10) , we assume an ansatz

$$A(\rho,z)=A_s(\rho)e^{-i\frac{S}{2}z}, \tag{2.2.11}$$

where S is a real constant and A_s is real. Without loss of generality, however, we may set $S=0$ by absorbing it into Combining (2.2.9) and (2.2.10) we have

$$\frac{1}{\rho}\frac{d}{d\rho}\left(\rho\frac{dA}{d\rho}\right)+\sigma A-\theta\left(1+\frac{1}{\rho}\frac{d}{d\rho}\left(\rho\frac{d\gamma}{d\rho}\right)\right)\frac{A}{\gamma}=0. \tag{2.2.12}$$

Note that $\gamma=\sqrt{1+A^2}$. We first consider the case where cavitation does not occur. Noting that $d\gamma/d\rho=(A/\gamma)dA/d\rho$ and that

$$\frac{1}{\rho}\frac{d}{d\rho}\left(\rho\frac{d\gamma}{d\rho}\right)=\frac{1}{\rho}\left[\frac{A}{\gamma}\frac{d}{d\rho}\left(\rho\frac{dA}{d\rho}\right)+\rho\frac{dA}{d\rho}\frac{d}{d\rho}\left(\frac{A}{\gamma}\right)\right],$$

we may recast (2.2.12) as

$$\frac{1}{\rho\gamma}\frac{d}{d\rho}\left(\frac{\rho}{\gamma}\frac{dA}{d\rho}\right)+\left(\sigma-\frac{1}{\gamma}\right)A=0. \tag{2.2.13}$$

We require that $A(\rho\to\infty)\to 0$ and that A must be evanescent at large ρ. Setting $\rho>>1$, (2.2.13) becomes

$$\frac{1}{\rho}\frac{d}{d\rho}\left(\rho\frac{dA}{d\rho}\right)+(\sigma-1)A=0. \tag{2.2.14}$$

The condition of evanescence places a restriction on σ. This may be seen by recognizing (2.2.14) as a zeroth-order Bessel differential equation. For evanescence we must have

$$\kappa^2 \equiv 1-\sigma > 0. \tag{2.2.15}$$

This gives us in the limit $\kappa\rho >> 1$, using C_∞ to denote an arbitrary constant,

$$A \sim C_\infty \sqrt{1/\kappa\rho}\, e^{-\kappa\rho}. \tag{2.2.16}$$

In the regions, if any, where cavitation occurs, we obtain from (2.2.12)

$$\frac{1}{\rho}\frac{d}{d\rho}\left(\rho\frac{dA}{d\rho}\right)+\sigma A = 0. \tag{2.2.17}$$

(2.2.17) is a zeroth-order Bessel differential equation, which solution is, assuming $\sigma > 0$,

$$A = A(0)J_0\left(\sigma^{1/2}\rho\right). \tag{2.2.18}$$

We may now solve for A by numerically solving (2.2.13) in regions of no cavitation, and using (2.2.18) in regions of cavitation. We require continuity and smoothness in our solution, so for transitions between (2.2.18) and (2.2.13) we impose the boundary conditions

$$A(\rho_+) = A(\rho_-),\ \frac{dA(\rho_+)}{d\rho} = \frac{dA(\rho_-)}{d\rho}, \tag{2.2.19}$$

where ρ_+ and ρ_- indicate positions on either side of the cavitation boundary. If cavitation never occurs, enforcing smoothness given the axisymmetric nature of the solution requires

$$\frac{dA(0)}{d\rho} = 0. \tag{2.2.20}$$

We perform our simulations using the shooting method employed by [36]. For each value of σ in the parameter space studied, we integrate (2.2.13) from an arbitrarily large ρ to $\rho = 0$. If at any point $\left(1+\nabla_t^2\sqrt{1+|A|^2}\right) < 0$, we use (2.2.18), matching boundary conditions with (2.2.19). If cavitation never occurs we integrate all the way to $\rho = 0$,

where (2.2.20) should hold for the solution to be valid. We specify initial conditions with (2.2.16), varying C_∞ until (2.2.19) and (2.2.20) are valid. As evident from its definition in (2.2.16), the value of σ controls the dispersion relation in the plasma:

$$\omega^2 = k^2c^2 + \sigma\omega_p^2 \tag{2.2.21}$$

Since we require $0 < \sigma < 1$ and focus on the case where $\omega/\omega_p >> 1$, we see that varying σ corresponds to a translation of the vacuum dispersion relation $\omega^2 = k^2c^2$ by a very small amount. We define the power of the beam as $P = \int_0^\infty |A(\rho)|^2 \rho d\rho$.

We repeat the simulations of [36] to obtain Fig. 2.2.1, from which it is evident that in this range of σ, decreasing the value of σ -- which implies, by (2.2.21), selecting a value of phase velocity $v_{ph} > c$ closer to c -- leads to a more tightly focused laser beam in the plasma, since the beam radius and the magnitude of the on-axis field $A(0)$ increases. As σ decreases (and $A(0)$ increases), the on-axis electron density $n(0)$ decreases toward 0 until $n(0) = 0$, i.e. cavitation occurs. Further decreases in σ lead to a widening of the electron cavity, as can be observed going from Fig. 2.2.1(c) to Fig. 2.2.1(d).

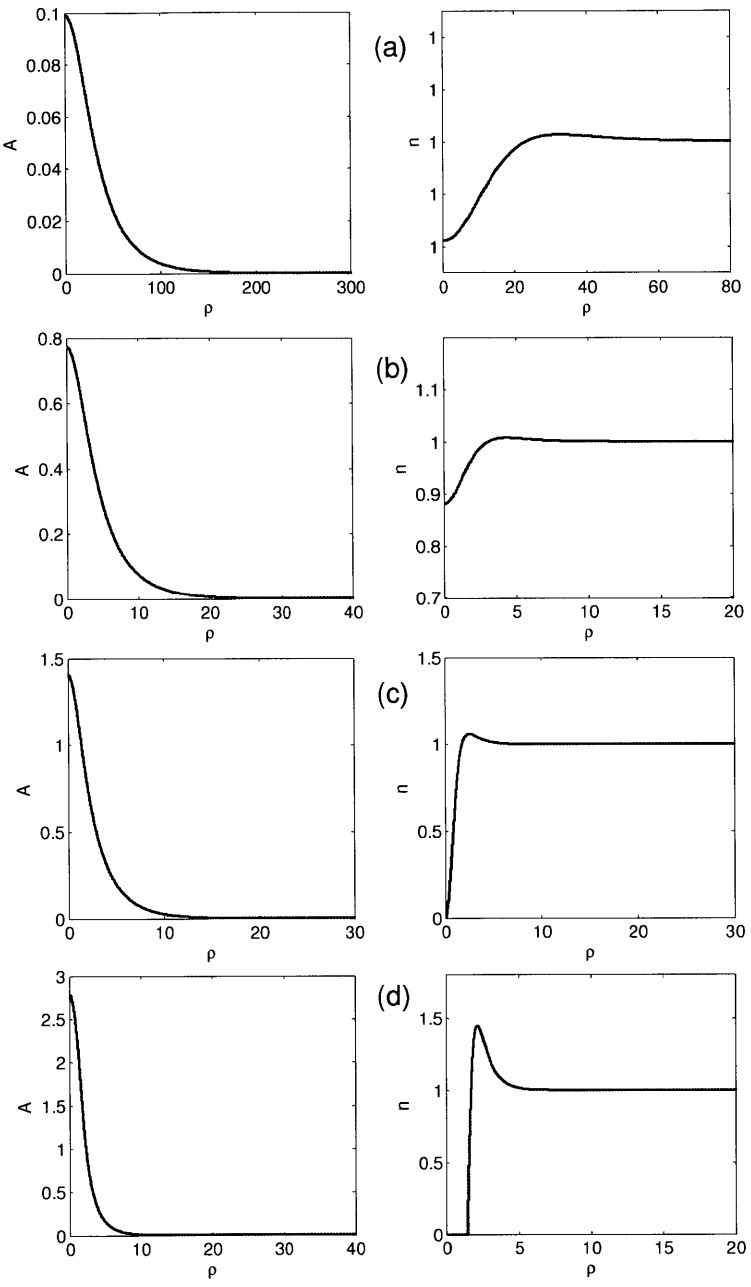

Fig. 2.2.1 Plots of normalized field amplitude A and normalized electron density n for (a) $\sigma = 0.999$, (b) $\sigma = 0.95$, (c) $\sigma = 0.8778$ and (d) $\sigma = 0.7$.

An asymptotic limit for $\rho_0\sqrt{\sigma}$ may be obtained in the limit that the beam power goes to infinity, where ρ_0 denotes the value of ρ at which cavitation occurs. To obtain this note that by definition

$$n(\rho_0) = 1 + \frac{1}{\rho}\frac{d}{d\rho}\left(\rho \frac{d}{d\rho}\sqrt{1 + A^2(\rho)}\right)_{\rho=\rho_0} = 0 \qquad (2.2.22)$$

For large A (which occurs when $\sigma \to 0$), (2.2.22) simplifies to

$$n(\rho_0) \approx \frac{1}{\rho}\frac{d}{d\rho}\left(\rho \frac{d}{d\rho}A(\rho)\right)_{\rho=\rho_0} = 0 \qquad (2.2.23)$$

With (2.2.18), this gives us

$$J_0\left(\rho_0 \sigma^{1/2}\right) \approx 0 \qquad (2.2.24)$$

So we may conclude that as $\sigma \to 0$, $\rho_0 \sigma^{1/2} \to 2.4048$, the first zero of the zeroth-order Bessel function, which the plot in Fig.2.2.2 confirms.

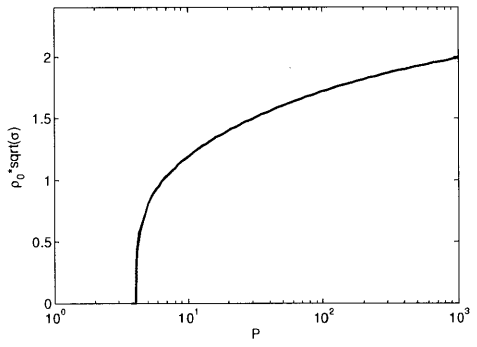

Fig. 2.2.2. Value of $\rho_0\sqrt{\sigma}$ vs. power

The studies of [36] only discuss the lowest order stationary states for various σ. In fact, the theory developed in [36] (which we have reviewed above) also predicts the existence of higher-order stationary states in the plasma. These higher-order stationary states may be shown to exist by noting that for a given σ, the shooting method of the previous section gives multiple solutions of C_∞, with larger values of C_∞ being associated with higher orders of solutions.

Fig. 2.2.3 shows how the field pattern and electron density of the fundamental mode studied in Fig. 2.2.1. We see that the field pattern indeed agrees with the plots in Fig. 2.2.1 (although the cases in Fig. 2.2.3 are at much higher powers), and that regardless of power it is made up of a single peak that decays as distance from the axis increases. In Fig. 2.2.4, we show the field patterns and electron densities of the second-order stationary states. The field patterns are now made up of two peaks: one at the axis and a smaller one off-axis. As expected, the field patterns of the third-order stationary states shown in Fig. 2.2.5 are made up of three peaks, the largest of which is on-axis and the smallest of which is the one farthest from the axis. Fig. 2.2.3-2.2.5 also show that the electron cavity for higher-order modes is larger. To find out how the size of the cavity scales with different orders of field patterns, we plot $\rho_0\sqrt{\sigma}$ vs. power, as we did for the fundamental mode in Fig. 2.2.2, for the second and third order modes in Fig. 2.2.6.

From Fig. 2.2.6, we see that the value of $\rho_0\sqrt{\sigma}$ for each order approaches an asymptotic value as power increases. Since (2.2.22)-(2.2.24) apply just as well to higher order beams, we may conclude that the asymptotic value for each higher order is simply given the next zero of the zeroth-order Bessel function $J_0\left(\rho_0\sigma^{1/2}\right)$ as one moves from the origin in the positive direction. Hence, as $\sigma \to 0$, $\rho_0\sigma^{1/2} \to 2.4048$, 5.5201, 8.6537 for the fundamental, second-order and third-order modes respectively, which we easily verify by studying Figs. 2.2.2 and 2.2.6. It is thus straightforward to see for each value of σ, an infinite number of solutions for $A(\rho)$ and $n(\rho)$ exist, each one corresponding to a particular zero of $J_0\left(\rho_0\sigma^{1/2}\right)$.

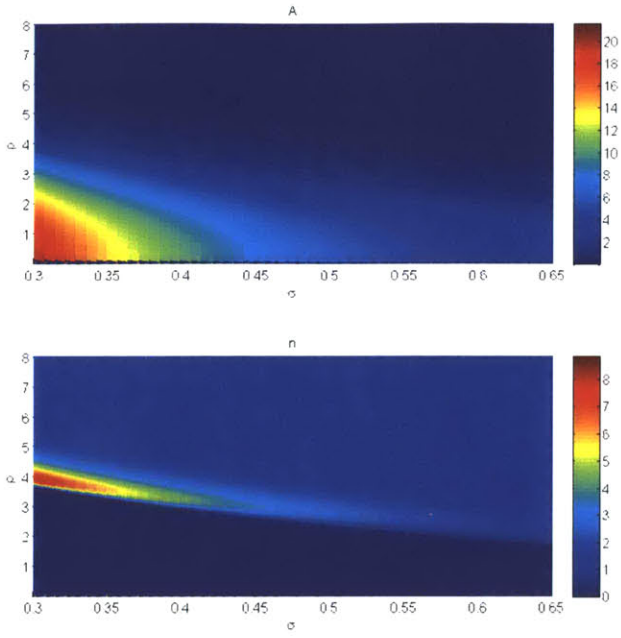

Fig. 2.2.3 Mesh plots of transverse field pattern A and electron density n for fundamental modes.

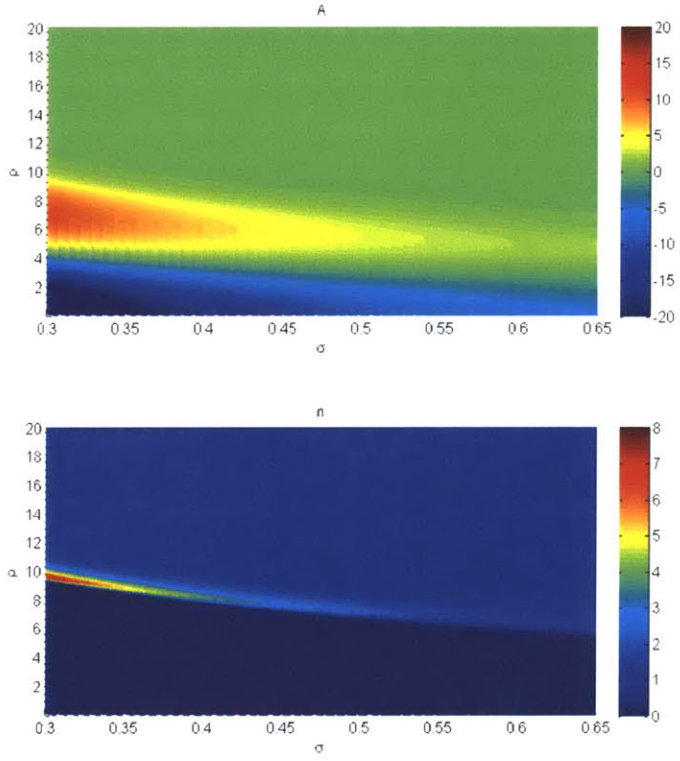

Fig. 2.2.4 Mesh plots of transverse field pattern A and electron density n for second-order modes

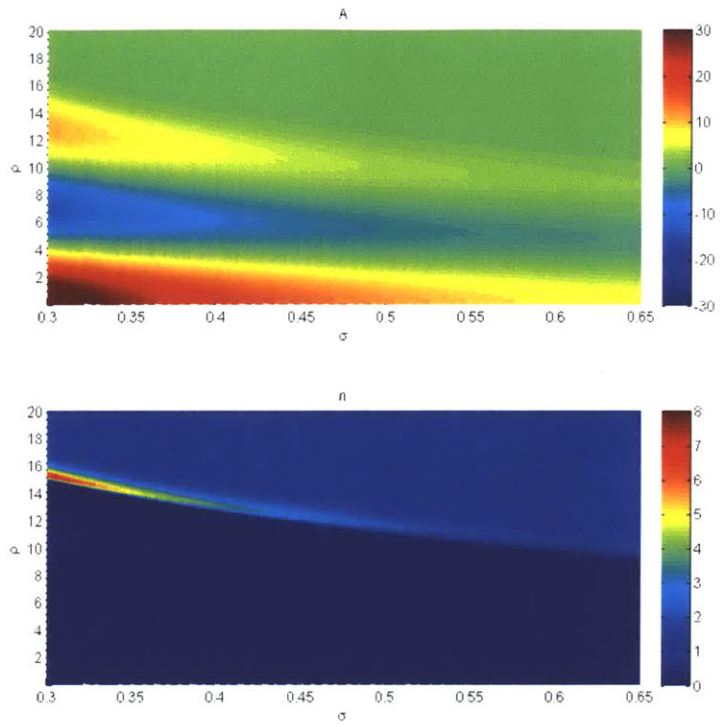

Fig. 2.2.5 Mesh plots of transverse field pattern A and electron density n for third-order modes

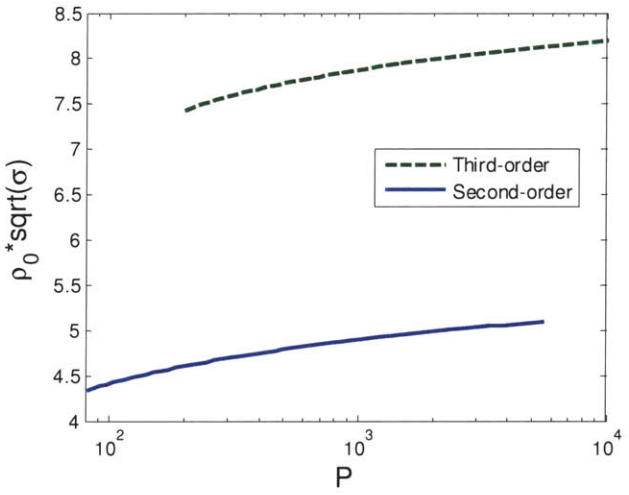

Fig. 2.2.6 Plots showing the asymptotic behavior of $\rho_0\sqrt{\sigma}$ at high powers for higher-order beams.

The sum of what the above analyses tell us is that an incident pulsed wave with certain combinations of peak power and transverse field pattern can propagate through initially uniform plasma with very little beam divergence, and with a phase velocity

determined by the value of σ to which the field pattern and peak power correspond. Self-focusing without any prior plasma channel-shaping may thus be achieved through the interaction between the driving laser beam and plasma that causes a redistribution of the electron density. Beyond a certain peak intensity of the driving beam, all electrons are expelled from the axis and electron cavitation occurs. We have shown that the theory of [36] also predicts the ability of the plasma to sustain higher-order beam modes. Higher-order modes are useful because they can increase the matched electron beam radius in wakefield acceleration, leading to increased charge and efficiency while maintaining low emittance of accelerated electron bunches [39].

3. Ponderomotive Acceleration of an Electron in Infinite Vacuum

In ponderomotive acceleration, electrons in vacuum gain energy (primarily) by the ponderomotive force, which is a longitudinally-directed force resulting from the combined effect of the transverse electric and magnetic fields on the electron. Among the variety of ponderomotive acceleration schemes conceived are inverse free electron laser (IFEL) acceleration [12, 13]; vacuum beat wave acceleration [15], in which the wiggler field of the IFEL is simply replaced by a second laser; high-intensity ponderomotive scattering [16-18], in which the electron is scattered away from the laser focus with a high escape energy; the capture and acceleration scenario [20], in which relativistic electrons are injected at an angle into the laser focus; and ionization of highly-charged ions near the laser pulse peak [22]. Experiments [13, 18, 23] have demonstrated that ponderomotive acceleration may be achieved in reality.

In this chapter, I study the ponderomotive acceleration of an electron in infinite vacuum by a pulsed linearly-polarized fundamental Gaussian beam, analyzing the case of an incident plane wave first for analytical insight (where I roughly follow the procedure of Hartemann et. al. [16]), before proceeding to model the Gaussian beam.

3.1 Electrodynamics of a single electron in a pulsed plane wave

Assuming that the effects of radiation reaction are negligible, the dynamics of the electron is governed by the Lorentz force equation:

$$\frac{d\vec{p}}{dt} = -e\left(\vec{E} + \vec{v} \times \vec{B}\right) \tag{3.1.1}$$

where m is the rest mass of the electron, e the absolute value of its charge, $\vec{p} = \gamma m\vec{v}$ its momentum, $\vec{v}$ its velocity and $\gamma \equiv 1/\sqrt{1-\beta^2} = \sqrt{\left(1+(\gamma\beta_x)^2+(\gamma\beta_y)^2\right)/\left(1-\beta_z^{\,2}\right)}$ $= \sqrt{1+(\gamma\beta)^2}$ is the Lorentz factor, with $\beta \equiv \left|\vec{\beta}\right|$ and $\vec{\beta} \equiv \vec{v}/c$. $\vec{E}$ is the electric field intensity and $\vec{B}$ the magnetic flux density. The total energy and kinetic energy of the electron are given by $G_T = \gamma mc^2$ and $G_K = (\gamma - 1)mc^2$ respectively. Using the retarded potentials, we substitute $\vec{E} = -\nabla\phi - \partial\vec{A}/\partial t$ and $\vec{B} = \nabla \times \vec{A}$, and apply vector identities to obtain from (3.1.1) (with subscripts x, y and z denoting components along the Cartesian coordinates)

$$\frac{d\left(\vec{p} - e\vec{A}\right)}{dt} = -e\left(-\nabla\phi + v_x\nabla A_x + v_y\nabla A_y + v_z\nabla A_z\right)$$

$$= -e\left(-\nabla\phi + \vec{v}\cdot\frac{\partial\vec{A}}{\partial x}\hat{x} + \vec{v}\cdot\frac{\partial\vec{A}}{\partial y}\hat{y} + \vec{v}\cdot\frac{\partial\vec{A}}{\partial z}\hat{z}\right) \qquad (3.1.2)$$

Taking the dot product of both sides of (3.1.1) with $\vec{v}$, we also have

$$\vec{v}\cdot\frac{d\vec{p}}{dt} = \frac{dG_T}{dt} = \frac{d\left(\gamma mc^2\right)}{dt} = -e\vec{v}\cdot\vec{E} \qquad (3.1.3)$$

Since we consider an incident plane wave, let $\vec{A} = A_x(\xi)\hat{x}$, $\xi \equiv \omega t - kz$, ω being the radian frequency and $k \equiv \omega/c$, and $a_x \equiv eA_x/mc$. We then have from (3.1.2) and (3.1.3)

$$\frac{d}{dt}(\gamma\beta_x - a_x) = 0 \qquad (3.1.4a)$$

$$\frac{d}{dt}(\gamma\beta_y) = 0 \qquad (3.1.4b)$$

$$\frac{d}{dt}(\gamma\beta_z) = -c\beta_x\frac{\partial a_x}{\partial z} \qquad (3.1.4c)$$

$$\frac{d\gamma}{dt} = \beta_x \frac{\partial a_x}{\partial t} \tag{3.1.4d}$$

Noting that $(-1/k)\partial a_x/\partial z = (1/\omega)\partial a_x/\partial t = \partial a_x/\partial \xi \Rightarrow \partial a_x/\partial z = (-1/c)\partial a_x/\partial t$, we combine (3.1.4c) and (3.1.4d) to obtain $d(\gamma(1-\beta_z))/dt = 0$, which gives us the invariant

$$\gamma(1-\beta_z) = \gamma_0(1-\beta_{z0}) \tag{3.1.5}$$

where an additional subscript 0 denotes the value of the variable at initial time. Solving (3.1.4a) gives us $\gamma\beta_x = \gamma_0\beta_{x0} + a_x$. (3.1.4c) may thus also be written as

$$\frac{d}{dt}(\gamma\beta_z) = -c\left(\frac{\gamma_0\beta_{x0} + a_x}{\gamma}\right)\frac{\partial a_x}{\partial z} = -c\left(\frac{\gamma_0\beta_{x0}}{\gamma}\right)\frac{\partial a_x}{\partial z} - c\frac{1}{2\gamma}\frac{\partial a_x^2}{\partial z} \tag{3.1.6}$$

where the term containing $\partial a_x^2/\partial z$ is proportional to the magnitude of the laser's intensity gradient and is referred to as the "ponderomotive force" or "nonlinear force", since the force depends nonlinearly on the electric field. This ponderomotive force is precisely the mechanism by which transverse components of an electromagnetic field accelerate electrons in the longitudinal direction in vacuum.

To summarize the solutions obtained from (3.1.4) and (3.1.5),

$$\gamma(\xi)\beta_x(\xi) = \gamma_0\beta_{x0} + a_x(\xi) \tag{3.1.7a}$$

$$\gamma(\xi)\beta_y(\xi) = \gamma_0\beta_{y0} \tag{3.1.7b}$$

$$\gamma(\xi)\beta_z(\xi) = \gamma(\xi) - \gamma_0(1-\beta_{z0}) \tag{3.1.7c}$$

$$\gamma(\xi) = \gamma_0\left(1 + \frac{2a_x(\xi)\gamma_0\beta_{x0} + a_x^2(\xi)}{2\gamma_0^2(1-\beta_{z0})}\right) \tag{3.1.7d}$$

where we have included the functional dependence for clarity. To solve for the particle's position $\vec{r}$ as a function of ξ, we note that $d\vec{r}/dt = (d\vec{r}/d\xi)(d\xi/dt) = \omega(1-\beta_z)(d\vec{r}/d\xi)$,

where $r\vec{r} = x\vec{x} + y\vec{y} + z\vec{z}$. Hence, $d(k\vec{r})/d\xi = \gamma(\xi)\vec{\beta}(\xi)/(\gamma_0(1-\beta_{z0}))$, which can be solved numerically for $k\vec{r}$ once initial conditions and $a_x(\xi)$ have been specified.

If we let $a_x(\xi) = a_0\cos(\xi)\operatorname{sech}(\xi/\xi_0)$ and set $\xi_0 = 14$, $\gamma_0 = 10$, $\beta_{x0} = \beta_{y0} = 0$, $a_0 = 2$, we get the plots for $a_x(\xi)$, $kx(\xi)$ and $kz(\xi)$ and $\gamma(\xi)$ in Fig. 3.1.1. As a guide to what fields and intensities are involved here, one should note that 1) for $\lambda = 0.8\mu\text{m}$, $a_0 = 1$ corresponds to a transverse electric field amplitude of $E_0 \approx 4\times10^{12}\,\text{V/m}$ and a root-mean-squared intensity of $S_{rms} \equiv E_0^2/2\eta_0 \approx 2\times10^{18}\,\text{W/cm}^2$ (η_0 is the vacuum wave impedance), and 2) $E_0 \propto a_0/\lambda$, $S_{rms} \propto (a_0/\lambda)^2$. Note that time increases linearly with ξ, the carrier phase at which the electron is located.

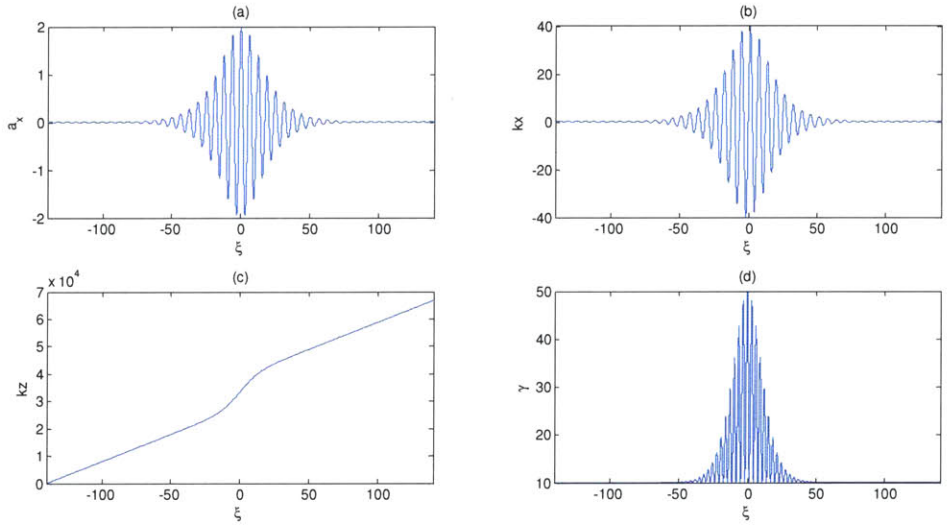

Fig. 3.1.1: Plots of a) normalized field amplitude, b) normalized transverse displacement, c) normalized longitudinal displacement and d) normalized electron energy vs. ξ for an incident plane wave with $\xi_0 = 14$, $\gamma_0 = 10$, $\beta_{x0} = \beta_{y0} = 0$, $a_0 = 2$.

In Fig. 3.1.1d, we see that the energy of the electron infinitely far in the past and infinitely far in the future are equal. The electron is thus not able to gain net energy from a pulsed plane wave. With a pulsed Gaussian beam, however, we will see in the next

section that the position-dependent spatial envelope of the beam allows the electron to gain significant energy from the laser-electron interaction.

Fig.3.1.1b shows that the pulse's oscillating field (Fig. 3.1.1a) causes the electron to oscillate similarly in the transverse direction as the pulse passes over the electron. The electron's "quiver amplitude", which is the maximum amplitude of its transverse motion, can be a source of concern in the production of well-collimated electron beams. This is because one would expect the electron to be expelled at a large angle with respect to the beam axis if the quiver amplitude becomes comparable to or greater than the laser beam radius. According to this argument, we may estimate the threshold for wide-angle scattering by equating maximum quiver amplitude x_0 and beam waist radius w_0. For the case $\beta_{x0} = \beta_{y0} = 0$, $x_0 = a_0\gamma_0(1+\beta_0)/k$. This corresponds to a threshold amplitude a_{th} of

$$a_{th} \approx \frac{w_0 k}{\gamma_0(1+\beta_0)} \approx \frac{w_0 k}{2\gamma_0} \text{ (for } \beta_{x0} = \beta_{y0} = 0) \tag{3.1.8}$$

where the rightmost equality in a_{th} applies for $\beta_{z0} \approx 1$. Note that [16] mistakenly argues that (3.1.8) gives the threshold for net electron acceleration. We see in the next section that significant net electron acceleration may be obtained with $a_0 < a_{th}$, which is in fact desirable because it favors a small scattering angle for the accelerated electron.

3.2 Ponderomotive acceleration of an electron in infinite vacuum by a pulsed linearly-polarized Gaussian beam

A pulsed linearly-polarized Gaussian beam is given in the Lorentz gauge by the complex vector potential $\vec{A} = \hat{x}A_0 f e^{-f\rho^2} e^{j(\xi+\psi_0)} \text{sech}((\xi + kz_i)/\xi_0)$, where x, y, z are the Cartesian coordinates and $\hat{x}, \hat{y}, \hat{z}$ the corresponding unit vectors; $j \equiv \sqrt{-1}$; $\rho \equiv r/w_0$;

$r \equiv \sqrt{x^2 + y^2}$; $f \equiv j/(j+(z/z_0))$; $\xi \equiv \omega t - kz$; $z_0 \equiv \pi {w_0}^2/\lambda$ is the Rayleigh range; w_0 is the beam waist radius; λ is the carrier wavelength (i.e. the central wavelength of the pulse); $k \equiv 2\pi/\lambda$; $\omega = kc$ is the angular carrier frequency; z_i is the pulse's initial position; ψ_0 is the carrier phase constant; ξ_0 is a parameter related to the pulse duration. One may easily verify that $\vec{A}$ satisfies the paraxial wave approximation as long as w_0 and ξ_0 are large enough [38]. In the $y = 0$ plane, one finds corresponding electromagnetic fields of the approximate form:

$$E_x = \sqrt{\frac{2\eta_0 P}{\pi\left(w_0/\sqrt{2}\right)^2}}\sqrt{L}e^{-\frac{x^2}{w_0^2}L}\sin(\psi)\operatorname{sech}\left(\frac{\xi + kz_i}{\xi_0}\right) \tag{3.2.1a}$$

$$B_y = \frac{E_x}{c} \tag{3.2.1b}$$

$$E_z = \sqrt{\frac{2\eta_0 P}{\pi\left(w_0/\sqrt{2}\right)^2}}\frac{L}{z_0}e^{-\frac{x^2}{w_0^2}L}\cos\left(\psi + \tan^{-1}\left(\frac{z}{z_0}\right)\right)\operatorname{sech}\left(\frac{\xi + kz_i}{\xi_0}\right) \tag{3.2.1c}$$

with all other components negligible. $\eta_0 \cong 120\pi\,\Omega$ is the vacuum wave impedance, c the speed of light in vacuum, P the peak pulse power , $\psi \equiv \xi + \tan^{-1}\left(\frac{z}{z_0}\right) - \frac{x^2}{w_0^2}L\frac{z}{z_0} + \psi_0$ and $L \equiv 1/\left(1+(z/z_0)^2\right)$. From (3.1.1) and (3.1.3) we obtain:

$$\frac{d(\gamma\beta_x)}{dt} = -\frac{e}{mc}E_x(1-\beta_z) \tag{3.2.2a}$$

$$\frac{d(\gamma\beta_z)}{dt} = -\frac{e}{mc}(E_z + \beta_x E_x) \tag{3.2.2b}$$

$$\frac{d\gamma}{dt} = -\frac{e}{mc}(\beta_x E_x + \beta_z E_z) \tag{3.2.2c}$$

where the variation in $\gamma\beta_y$ is 0. Combining (3.2.2b) and (3.2.2c) we find

$$\frac{d\gamma(1-\beta_z)}{dt} = \frac{e}{mc} E_z(1-\beta_z) \tag{3.2.3}$$

(3.2.3) tells us that unlike the plane wave case in section 3.1, the Gaussian beam case does not conserve $\gamma(1-\beta_z)$ due to the presence of the longitudinal component of the electric field, which in turn arises from focusing (i.e. Gauss's law, $\nabla_T \cdot \vec{E} = -\partial E_z/\partial z$, requires a non-zero E_z due to the non-zero transverse divergence of the transverse electric field). We may substitute (3.2.1) into (3.2.2), introducing normalizations $X \equiv kx$, $Z \equiv kz$ ($Z_i \equiv kz_i$), $\varepsilon_d \equiv \lambda/\pi w_0$ and $T \equiv \omega t$ to obtain

$$\frac{d(\gamma\beta_x)}{dT} = -V_0 e^{-\left(\frac{\varepsilon_d}{2}X\right)^2 L}(1-\beta_z)\sqrt{L}\sin(\psi)\operatorname{sech}\left(\frac{\xi+Z_i}{\xi_0}\right) \tag{3.2.4a}$$

$$\frac{d(\gamma\beta_z)}{dT} = -V_0 e^{-\left(\frac{\varepsilon_d}{2}X\right)^2 L}\left\{X\frac{\varepsilon_d^2}{2}L\cos(\psi_z) + \beta_x\sqrt{L}\sin(\psi)\right\}\operatorname{sech}\left(\frac{\xi+Z_i}{\xi_0}\right) \tag{3.2.4b}$$

where $\psi \equiv \xi + \tan^{-1}(\varepsilon_d^2 Z/2) - (\varepsilon_d X/2)^2 L(\varepsilon_d^2 Z/2) + \psi_0$, $\psi_z \equiv \psi + \tan^{-1}(\varepsilon_d^2 Z/2)$, $\xi \equiv T - Z$, $V_0 \equiv \sqrt{4\eta_0 P/\pi}e\varepsilon_d/2mc^2$, $L \equiv 1/(1+(\varepsilon_d^2 Z/2))^2$. Together with the ordinary differential equations $dX/dT = \beta_x$ and $dZ/dT = \beta_z$, (3.2.4) may be solved for $\gamma\beta_z$, $\gamma\beta_x$, X and Z as a function of time after specifying laser parameters ξ_0, P, ε_d, ψ_0 and electron parameters $X(0)$, $Z(0)$, $\beta_x(0)$, $\beta_z(0)$. We have not included Z_i as a degree of freedom because we always effectively set $Z_i \to -\infty$ (i.e. the electron begins in field-free vacuum). The simulation is terminated only after the electron is again effectively in field-free vacuum. A schematic of the simulation is shown in Fig. 3.2.1.

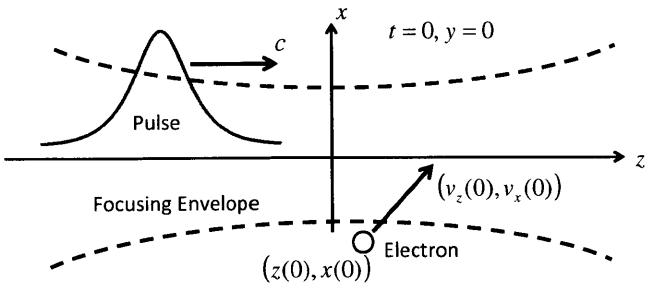

Fig. 3.2.1: Simulation schematic for electron acceleration by a pulsed linearly-polarized Gaussian beam.

Instead of specifying $(Z(0), X(0))$, it is convenient to specify (D_z, D_x), which we call the "protracted collision position" and define as the (normalized) position where the electron's z-position would coincide with that of the pulse peak if the electron were to always travel at its initial velocity $(v_z(0), v_x(0))$. For values of (D_z, D_x) far enough from the laser focus such that the electron always experiences a negligibly small electric field (resulting in little change in the electron's velocity from its initial value), (D_z, D_x) approximates the actual position where electron and pulse peak coincide, hence our name for it. We thus have the relations

$$Z_i = \frac{1}{\beta_z(0)}\left(Z(0) - D_z\left(1 - \beta_z(0)\right)\right) \tag{3.2.5a}$$

$$X(0) = D_x - \beta_x(0)\left(D_z - Z_i\right) \tag{3.2.5b}$$

Note that our problem is independent of carrier wavelength λ and so the solutions may be scaled to any λ. As an alternative to specifying $(\beta_z(0), \beta_x(0))$, we may specify $\theta \equiv \tan^{-1}\left(\beta_x(0)/\beta_z(0)\right)$ and $\gamma(0) = \gamma_0$. We also define $\alpha \equiv \lim_{t\to\infty} \tan^{-1}\left(\beta_x/\beta_z\right)$ to be the electron's final scattering angle, defined as the angle the electron makes with the beam axis after the pulse has passed over the electron completely. The relationship between pulse energy E_{pulse} and peak pulse power P may be computed as

$$E_{pulse} = \frac{1}{\mu_0}\int_{-\infty}^{\infty} dt \int_{-\infty}^{\infty} dx \int_{-\infty}^{\infty} dy \vec{E}(x, y, z = 0, t) \times \vec{B}(x, y, z = 0, t) \cdot \hat{z} \approx P \frac{2\xi_0}{\omega} \quad (3.2.6)$$

where μ_0 is the permeability of free space. Following the convention of [29], we define pulse duration τ as

$$\tau = \frac{\xi_0}{\omega} \operatorname{sech}^{-1}(\exp(-1)) \quad (3.2.7)$$

Note that by this definition, τ also approximates the full-width half maximum intensity pulse duration of the pulse.

We now run a simulation under the conditions of Fig. 3.1.1 ($\xi_0 = 14$, $\gamma(0) = 10$, $\beta_x(0) = \beta_y(0) = 0$, $a_0 = 2$) to make a comparison with the plane wave case. Here, $a_0 = e\sqrt{4\eta_0 P/(\pi\omega^2 w_0^2)}/(mc)$, so to obtain Fig. 3.1.1's conditions for $\lambda = 0.8\mu\text{m}$, we can choose $P = 84.2\text{TW}$ and $w_0 = 25\mu\text{m}$ for a pulse energy $E_{pulse} = 1\text{J}$. The simulation results are shown in Fig. 3.2.2.

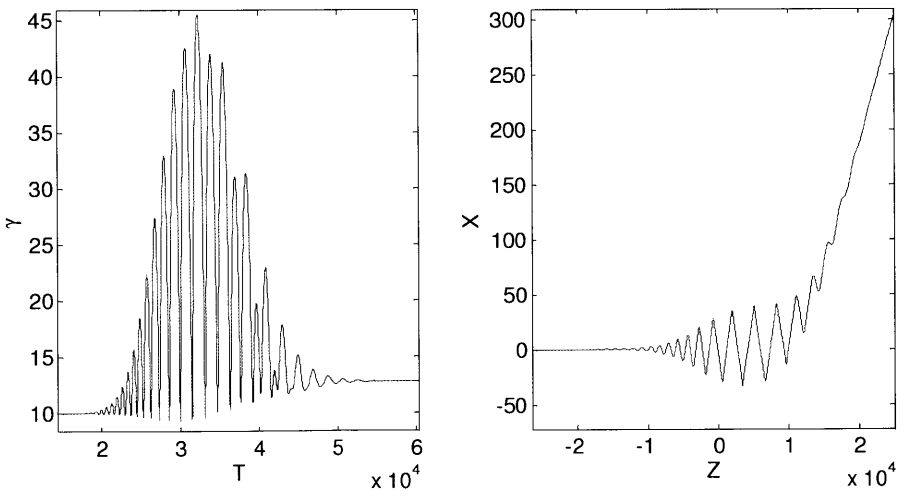

Fig. 3.2.2: Plots of a) normalized electron energy vs. normalized time, b) normalized transverse displacement vs. normalized longitudinal displacement for $\xi_0 = 14$, $\gamma_0 = 10$, $\beta_x(0) = \beta_y(0) = 0$, $a_0 = 2$, as in Fig. 3.1.1. We have chosen $\lambda = 0.8\mu\text{m}$, $P = 84.2\text{TW}$, $w_0 = 25\mu\text{m}$, $D_x = D_z = 0$, $\psi_0 = -\pi/2$.

Fig. 3.2.2a is reminiscent of Fig. 3.1.1d, except the spatial dependence of the focused beam introduces an asymmetry that results in a non-zero net transfer of energy from laser pulse to electron. Fig. 3.2.2b shows that after some wiggling, the electron departs at an angle to the beam axis. Our computations give us $\alpha = 1.345^0$. That α is relatively small here is not surprising, since by (3.1.8), the threshold for wide-angle scattering is $a_{th} = 9.82 > a_0$. Note that (3.1.8) may be cast for a Gaussian beam as

$$P_{th} \approx \frac{\pi^5}{\gamma_0^2}\left(\frac{\varepsilon_0 m^2 c^5}{e^2}\right)\left(\frac{w_0}{\lambda}\right)^4\left(\frac{2}{1+\beta_z(0)}\right)^2 \approx \frac{0.21}{\gamma_0^2}\left(\frac{w_0}{\lambda}\right)^4 \text{TW} \qquad (3.2.8)$$

where the rightmost expression applies for the case $\beta_z(0) \approx 1$.

We may increase a_0 for fixed laser peak power, pulse duration and pulse energy by decreasing w_0 (focusing more tightly), which also decreases a_{th}. The results of focusing by different amounts are shown in Fig. 3.2.3.

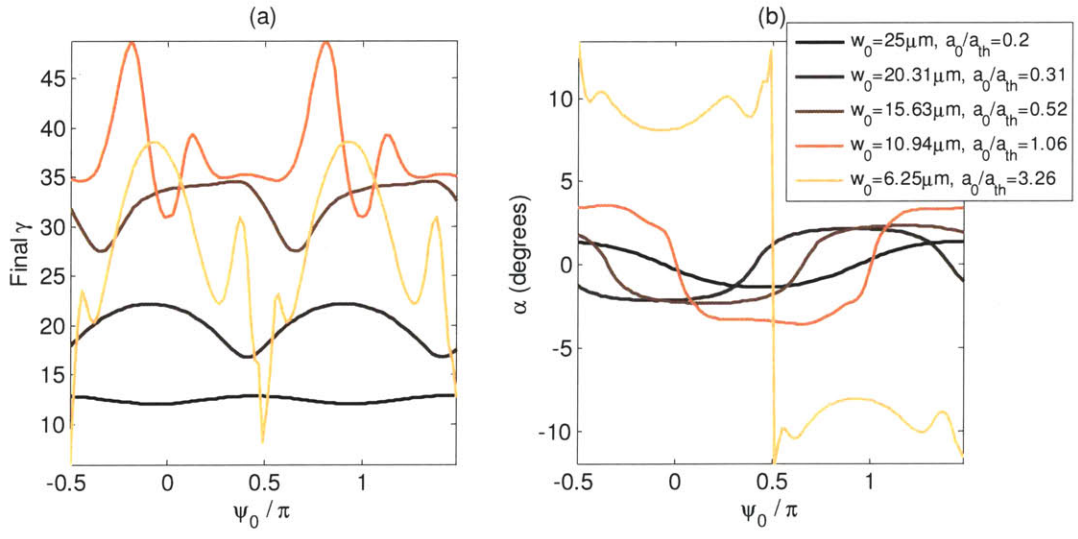

Fig. 3.2.3: Plots of a) Final γ vs. ψ_0 and b) Scattering angle α vs. ψ_0 for various w_0. with $\xi_0 = 14$, $\gamma_0 = 10$, $\beta_x(0) = \beta_y(0) = 0$. We have chosen $\lambda = 0.8\mu\text{m}$, $P = 84.2\text{TW}$, $D_x = D_z = 0$.

From Fig. 3.2.3, we see that under the given conditions, focusing more and more tightly causes the net energy gained to increase and α to increase only gradually until about $a_0/a_{th}=1$, when α increases drastically and the net energy gained decreases with further focusing. The phase dependence of the final energy gain also seems more phase-sensitive for $a_0/a_{th}>1$. For maximum net energy transfer and a relatively small scattering angle, the condition

$$\frac{a_0}{a_{th}}=\frac{2\gamma_0 e}{m}\left(\frac{\varepsilon_d}{2c}\right)^2\sqrt{\frac{4\eta_0 P}{\pi}}\sim 1 \qquad (3.2.9)$$

appears to be desirable in the case studied here. This suggests that to keep the final scattering angle small, an increase in P or γ_0 requires a corresponding increase in ε_d (i.e. a decrease in focusing), at least for the $D_x=D_z=0$, $\beta_x(0)=\beta_y(0)=0$ case. In the next chapter, we study an electron acceleration scheme in vacuum where electrons on the beam axis are not scattered at an angle to the axis, and which thus appears to favor the production of collimated electron beams.

4. Direct Acceleration of an Electron in Infinite Vacuum by a Radially-Polarized Beam

4.1 Introduction

In this chapter, I study the direct acceleration of a free electron in infinite vacuum along the axis of a pulsed radially-polarized laser beam. All optimizations are carried out in view of maximizing net energy transfer from laser pulse to electron. I begin by studying the initially stationary electron. There has been some interest [26-28,31,32] in the scenario of electrons born (for instance, by ionization) in the path of the laser pulse, and a recent study by Fortin et. al. [28] showed that an electron can reach the high-intensity cycles of the pulse without having been released by photoionization near the pulse peak. The study also concluded that the optimal beam waist at petawatt peak powers lies well within the paraxial wave regime. The latter conclusion, however, is true only for an initially stationary electron required to start at the laser focus. I show that after including the electron's initial position in the optimization space, one in fact achieves maximum acceleration with the most tightly-focused laser.

I also study the acceleration of electrons with non-zero initial velocities. These electrons (which I call "pre-accelerated electrons") are injected into the laser beam ahead of the pulse and may be the output of a preceding acceleration stage. I show that net energy gain can be much greater for a pre-accelerated electron than for an initially stationary one. In particular, the net energy gain of an initially relativistic electron may exceed more than half the theoretical energy gain limit (derived in [28]), which is not possible with an initially stationary electron in the parameter space studied. The *de facto* energy gain limit (of half the theoretical energy gain limit) argued by Fortin et. al. [28]

for the initially stationary electron may thus be surpassed with the pre-accelerated electron. Based on my simulation results, I also hypothesize that substantial electron acceleration cannot be achieved if the electron's initial kinetic energy greatly exceeds the laser's theoretical gain limit.

Prior to the study in [29], most studies focused on petawatt powers and beyond. By extending our parameter space to include powers as low as 5 TW, I show that substantial acceleration can already be achieved with laser peak powers of a few terawatts. In particular, I give an example in which a 5 TW pulse, either 7.5 fs or 15 fs in pulse duration, accelerates an electron from a kinetic energy of 10 MeV to a kinetic energy of about 50 MeV; and another example in which a two-stage accelerator employing a 10 TW, 10 fs pulse in each stage accelerates an initially stationary electron to a final kinetic energy of about 36 MeV. These electron energies are already sufficient for applications like the production of hard X-rays via inverse Compton scattering [33].

This chapter is organized as follows: In Section 4.2, I discuss the theoretical and technical aspects of our simulations; in Section 4.3, I study the acceleration of an initially stationary electron; in Section 4.4, I study the acceleration of a pre-accelerated electron.

4.2 Theory of direct acceleration by a pulsed radially-polarized laser beam

The physical scenario we study is the following: A free electron, initially at rest or moving in field-free vacuum, is overtaken by the pulse of a radially-polarized laser beam that exchanges energy with the electron purely via the laser's on-axis, longitudinal electric field (i.e. via direct acceleration). The pulse eventually overtakes the electron, leaving the electron once again in field-free vacuum, with a velocity generally different from what it had before. The free electron may have been introduced either by ionization

of a target in the path of the pulse, as in [32], or by a preceding acceleration stage. To compute the net energy gain of the electron, we need a description of the laser pulse and equations to model the electron's motion.

Using the method of [38], we may derive the electric field $\vec{E}$ and magnetic flux density $\vec{B}$ for a pulsed radially-polarized laser beam in vacuum under the paraxial wave approximation:

$$\vec{E}(r,z,t) = \mathrm{Re}\left\{\tilde{E}(r,z)e^{j(\xi+\psi_0)}\mathrm{sech}\left(\frac{\xi + kz_i}{\xi_0}\right)\right\}, \quad \vec{B}(r,z,t) = \hat{\phi}\frac{1}{c}\vec{E}(r,z,t)\cdot\hat{r}, \qquad (4.2.1)$$

where

$$\tilde{E}(r,z) \equiv f^2\rho e^{-f\rho^2}\sqrt{\frac{8\eta_0 P}{\pi w_0{}^2}}\left[\hat{r} - \hat{z}\frac{2j}{kr}\left(1 - f\rho^2\right)\right], \quad \tilde{B}(r,z) \equiv \hat{\phi}\frac{1}{c}\tilde{E}(r,z)\cdot\hat{r}, \qquad (4.2.2)$$

r,ϕ,z are the cylindrical coordinates and $\hat{r},\hat{\phi},\hat{z}$ the corresponding unit vectors; $j \equiv \sqrt{-1}$; $f \equiv j/\left(j + (z/z_0)\right)$; $\rho \equiv r/w_0$; $\xi \equiv \omega t - kz$; $z_0 \equiv \pi w_0{}^2/\lambda$ is the Rayleigh range; w_0 is the beam waist radius; λ is the carrier wavelength (i.e. the central wavelength of the pulse); $k \equiv 2\pi/\lambda$; $\omega = kc$ is the angular carrier frequency; $\eta_0 \cong 120\pi\,\Omega$ is the vacuum wave impedance; c is the speed of light in vacuum; z_i is the pulse's initial position; ψ_0 is the carrier phase constant; ξ_0 is a parameter related to the pulse duration; P is the peak power of the pulse:

$$P = \frac{1}{2\mu_0}\int_0^\infty dr 2\pi r\,\mathrm{Re}\left\{\tilde{E}(r,0)\times\tilde{B}^*(r,0)\cdot\hat{z}\right\} \qquad (4.2.3)$$

where μ_0 is the permeability of free space. By choosing values of ξ_0 such that the time variation of the sech pulse envelope is large compared to the time variation of the carrier and using Eq. (3), we may compute the pulse energy E_{pulse} as

$$E_{pulse} = \frac{1}{\mu_0}\int_{-\infty}^{\infty} dt \int_0^{\infty} dr 2\pi r \vec{E}(r,0,t) \times \vec{B}(r,0,t) \cdot \hat{z} \approx P \int_{-\infty}^{\infty} dt \operatorname{sech}^2\left(\frac{\omega t + kz_i}{\xi_0}\right) = P\frac{2\xi_0}{\omega} \quad (4.2.4)$$

We have chosen to model our pulse with a sech envelope because this allows Eq. (4.2.1) to satisfy the Maxwell equations in the paraxial wave approximation for $\xi_0 >> 1$. As shown in [40], the same cannot be said for other choices of pulse shapes. In particular, using a Gaussian pulse $\exp\left(-(\xi + kz_i)^2/\xi_0^{\,2}\right)$, instead of $\operatorname{sech}((\xi + kz_i)/\xi_0)$, would cause Eq. (1) to violate the Maxwell equations at large values of $(\xi + kz_i)$ (i.e. at the tails of the pulse). However, as will be seen in the next section, we are able to reproduce the results of [28] – which used a Gaussian pulse – with our model, showing that the former approach does not suffer much in accuracy in the parameter space of [28]. This is because the electrodynamics for most cases in [28] is primarily influenced by fields close to the pulse peak, where both Gaussian and sech representations are accurate.

Following the convention of [28], we define the pulse duration τ to be the single-sided $\exp(-1)$ duration of the pulse:

$$\tau = \frac{\xi_0}{\omega}\operatorname{sech}^{-1}(\exp(-1)). \quad (4.2.5)$$

Eq. (4.2.1) thus uniquely defines a pulsed radially-polarized laser beam after we specify six parameters: carrier wavelength λ, carrier phase constant ψ_0, beam waist radius w_0, initial pulse position z_i, peak power P and pulse duration τ. The pulse

energy E_{pulse} and parameter ξ_0 are then fixed by equations (4.2.4) and (4.2.5) respectively.

The electrodynamics of an electron in an electromagnetic field, ignoring radiative reaction, is described by the Newton-Lorentz equation of motion

$$\frac{d\vec{p}}{dt} = \frac{d(\gamma m\vec{v})}{dt} = -e\left(\vec{E} + \vec{v} \times \vec{B}\right), \tag{4.2.6}$$

where r, ϕ, z in the variables of Eq. (4.2.6) now denote the coordinates of the electron's position, m is the rest mass of the electron, e the absolute value of its charge, $\vec{p}$ its momentum, $\vec{v}$ its velocity and $\gamma \equiv 1/\sqrt{1-\beta^2}$ is the Lorentz factor, with $\beta \equiv |\vec{\beta}|$ and $\vec{\beta} \equiv \vec{v}/c$. The total energy and kinetic energy of the electron are given by $E_t = \gamma mc^2$ and $E_K = (\gamma - 1)mc^2$ respectively.

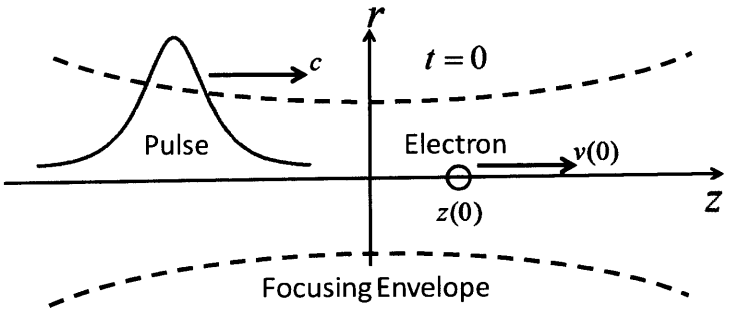

Fig. 4.2.1. Schematic of simulations at initial time. The electron begins in field-free vacuum.

We consider an electron initially ($t = 0$) on the beam axis ($r = 0$) of the laser at $z = z(0)$ (Fig. 4.2.1), moving in the longitudinal direction with velocity $\vec{v}(0) = v(0)\hat{z}$. The electron may be initially at rest ($v(0) = 0$) or moving ($v(0) > 0$; we do not consider $v(0) < 0$). The former case is the subject of Section 4.2.3, whereas the latter is the subject of Section 4.2.4. In all cases, we are interested in the net energy the electron extracts from

the laser field as the pulse propagates from a position (effectively) infinitely far behind the electron to a position (effectively) infinitely far in front of the electron. We do not limit the interaction distance by use of any additional optics. We also confine our attention to forward scattering cases (i.e. the electron's final velocity is in the direction of pulse propagation $+z$).

Setting $r = 0$ in Eq. (1), we have $\vec{E} = E_z \hat{z}$ and $\vec{B} = 0$, where

$$E_z = \left[\frac{1/z_0}{1+(z/z_0)^2} \sqrt{\frac{8\eta_0 P}{\pi}} \right] \sin\left(\omega t - kz + 2\tan^{-1}\left(\frac{z}{z_0}\right) + \psi_0 \right) \operatorname{sech}\left(\frac{\omega t - k(z - z_i)}{\xi_0} \right) \quad (4.2.7)$$

Eq. (4.2.7) may be seen as the product of three parts: the *field amplitude*, given by the square bracketed factor, which is a Lorentzian in z; the *continuous wave (CW) carrier*, given by the $\sin(\cdot)$ factor; and the *pulse envelope*, given by the $\operatorname{sech}(\cdot)$ factor. The sign of E_z is determined exclusively by that of the CW carrier. If the CW carrier is positive, meaning its argument is between 0 and π radians, an electron traveling in the $+z$ direction is in a *decelerating cycle* and loses energy to the field. If the CW carrier is negative, meaning its argument is between π and 2π radians, an electron traveling in the $+z$ direction is in an *accelerating cycle* and gains energy from the field. An on-axis electron with no initial transverse velocity component is confined to move along the beam axis (so $\vec{v}(t) = v(t)\hat{z}\ \forall t$, $r(t) = 0\ \forall t$). Simplifying (4.2.6), we obtain the equations

$$\frac{d\beta}{dt} = -\frac{eE_z}{\gamma^3 mc}, \quad \frac{dz}{dt} = v = c\beta. \quad (4.2.8)$$

Eq. (4.2.8) may be solved numerically for the electron's speed, and hence its energy, at any time. To do so, however, we must first specify the laser field (by specifying λ,

ψ_0, w_0, z_i, P and τ) as well as the electron's initial position $z(0)$ and speed $v(0)$. As mentioned, we always set z_i such that the pulse effectively begins infinitely far behind the electron. In addition, we fix $\lambda = 0.8\mu m$ throughout the paper, leaving us with a total of six dimensions over which to study or optimize the problem. Although we fix λ, our results may be readily scaled to obtain the results for any λ by nature of Eqs. (4.2.7) and (4.2.8), as we see in the next sub-section.

If we let $\mathrm{T} \equiv \omega t$, $\varsigma \equiv z / z_0$ (with $\varsigma_i \equiv z_i / z_0$) and $\kappa \equiv k z_0 = 2(\pi w_0 / \lambda)^2$, and apply Eq. (4.2.7), Eq. (4.2.8) may be cast in the form

$$\frac{d\beta}{d\mathrm{T}} = -\frac{e}{\gamma^3 mc^2}\left[\frac{1/\kappa}{1+\varsigma^2}\sqrt{\frac{8\eta_0 P}{\pi}}\right]\sin\left(\mathrm{T} - \kappa\varsigma + 2\tan^{-1}(\varsigma) + \psi_0\right)\mathrm{sech}\left(\frac{\mathrm{T} - \kappa(\varsigma - \varsigma_i)}{\xi_0}\right), \quad \frac{d\varsigma}{d\mathrm{T}} = \frac{\beta}{\kappa} \tag{4.2.9}$$

For given values of κ and ξ_0, Eq. (4.2.9) is completely independent of central wavelength λ. The results for any λ may thus be obtained from the results for $\lambda = 0.8\mu m$ by an appropriate scaling of beam waist w_0 and pulse duration τ. Note that κ determines the ratio w_0/λ and ξ_0 determines the number of cycles in the pulse envelope, regardless of λ. The scaling in t and z does not affect the maximum energy gain, only the optimal z_i.

By substituting Eqs. (4.2.1) and (4.2.2) into Eq. (4.2.6) and applying $\rho \equiv r / w_0$ along with the previous normalizations, it is straightforward to generalize our conclusion and see that for given values of κ and ξ_0, the electrodynamic equations are independent of λ even for the most general case where the electron is not necessarily on the beam axis. The acceleration of an (on-axis or otherwise) electron in infinite vacuum by a pulsed

radially-polarized laser beam thus depends on λ only through κ and ξ_0. An important consequence of this is that for a given peak power P, a larger pulse energy is required for exactly the same maximum acceleration at a larger λ if focusing (w_0/λ) remains constant, because the number of carrier cycles in the pulse envelope must also remain constant, leading to a longer pulse.

The Gouy phase shift term $2\tan^{-1}(z/z_0)$ in the argument of the CW carrier in Eq. (4.2.7) prevents any particle from remaining in a single cycle indefinitely. As a result, the energy that an electron can gain from a pulsed radially-polarized laser beam has a theoretical limit ΔE_{lim} that may be computed by considering an electron that (unrealistically) remains at the pulse peak and in one accelerating cycle from the focus to infinity (or from $-z_0$ to z_0, which gives the same result, just with a different ψ_0), as was done in [28]:

$$\Delta E_{\text{lim}} = \int_0^\infty dz \left[\frac{e/z_0}{1+(z/z_0)^2} \sqrt{\frac{8\eta_0 P}{\pi}} \right] \sin\left(2\tan^{-1}(z/z_0)\right) = e\sqrt{\frac{8\eta_0 P}{\pi}} \cong \sqrt{\frac{P}{[PW]}}[GeV] \quad (4.2.10)$$

where $P/[PW]$ refers to the laser peak power in petawatts. We will find it convenient to normalize our energy gain results by ΔE_{lim} afterwards.

We solve Eq. (4.2.8) numerically via the Adams-Bashforth-Moulton method (*ode113* of *Matlab*). In every case, we ensure that the pulse begins so far behind the electron that the latter is initially not affected by the laser field. By this we mean that any fluctuation in the electron's energy is at first (for at least a few tens of picoseconds) below an arbitrarily small value. We also terminate our simulations only after the electron's energy has

reached a steady state (equivalently, after electron position z has become so large that the Lorentzian field amplitude of Eq. (4.2.7) is negligibly small).

As discussed, Eq. (4.2.1) satisfies the Maxwell equations only for sufficiently large beam waists and pulse widths. To ensure the validity of our simulations, the smallest waist and pulse duration we consider are respectively $w_0 = 2\mu m$ and $\tau = 7.5 fs$, after the fashion of Fortin et. al. [28] and based on findings by Varin et. al. [31] that corrections to the paraxial radially-polarized laser beam are small or negligible for beam waists no smaller than $w_0 = 2\mu m$. For $\tau \geq 7.5 fs$, $\xi_0 > 10$, which at least approximately satisfies the requirement that $\xi_0 >> 1$.

4.3. Direct acceleration of an initially stationary electron

In [28], Fortin et. al. studied the case of a pulsed radially-polarized laser beam incident on an electron that was initially stationary at the laser focus. The authors concluded that, for the range of laser peak powers and pulse durations studied, the optimal laser focusing is in general not the tightest. This conclusion, however, is true only for electrons required to start at the laser focus (i.e. $z(0) = 0$). Given P, τ and w_0 in general, $z(0) = 0$ (or even slightly less than 0, as the authors suggest) is not the optimal initial position. We find after optimizing over ψ_0 - w_0 - $z(0)$ space that the optimal focusing is in fact the tightest.

In Fig. 4.3.1, we plot the maximum energy gain and optimal beam waist computed by optimizing over ψ_0 - w_0 space for $z(0) = 0$ (as in [28]). In Fig. 4.3.1(a), we also plot the maximum energy gain computed by optimizing over ψ_0 - w_0 - $z(0)$ space for $w_0 \geq 2$ μm (giving optimal $w_0 = 2$ μm). Our results for $z(0) = 0$ are clearly in good agreement with

those in [28] (slight differences may be attributed to our use of a different pulse shape). We see that a substantial increase in maximum energy gain occurs after including the $z(0)$ dimension in the optimization space. In fact, 15 fs and 20 fs pulses can approximately give us the energy gain that for $z(0) = 0$ is achievable only with 7.5 fs and 10 fs pulses respectively.

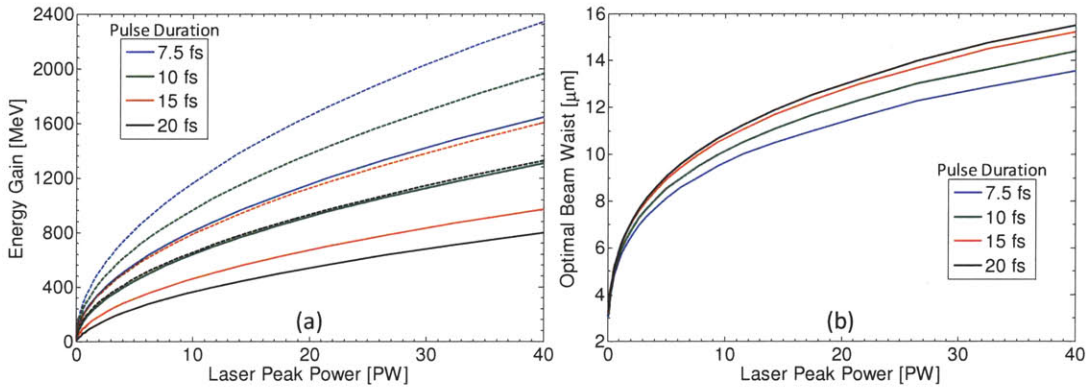

Fig. 4.3.1. (a) Maximum energy gain and (b) corresponding optimal beam waist vs. power P from 0.1 to 40 PW for various τ. All solid lines correspond to $z(0) = 0$. Dashed lines correspond to optimal $z(0)$ for $w_0 = 2$ μm (optimal waist). All cases shown correspond to forward scattering of the electron.

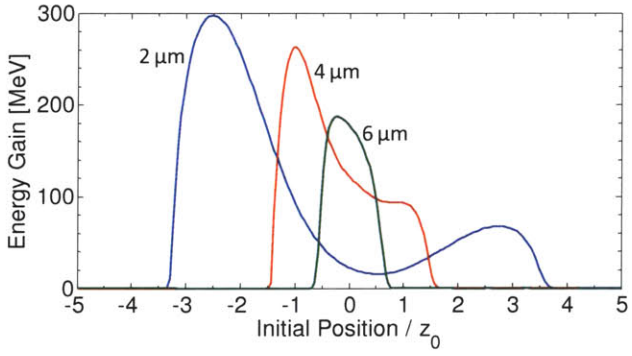

Fig. 4.3.2. Maximum energy gain vs. normalized $z(0)$ for $P = 1$ PW, $\tau = 10$ fs and various w_0. All cases shown correspond to forward scattering of the electron.

To illustrate how $z(0) = 0$ is not optimal in general, the energy gain (maximized over ψ_0 space) as a function of $z(0)$ normalized by z_0 for a 1 PW, 10 fs pulse is plotted for

various waists in Fig. 4.3.2. As can be seen, the optimal $z(0)$ approaches the focus as w_0 increases for given P and τ, but in general may be quite a distance behind the focus.

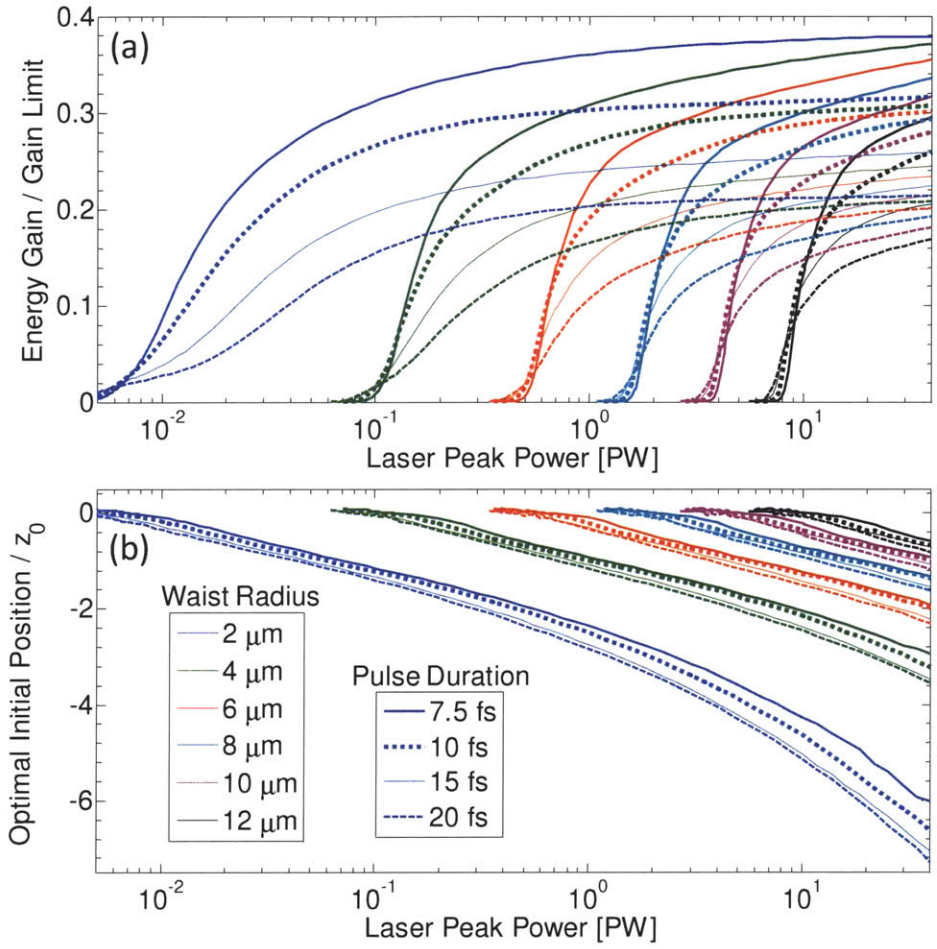

Fig. 4.3.3. (a) Normalized maximum energy gain and (b) corresponding normalized optimal initial position vs. P from 5 TW to 40 PW for various w_0 and τ. All cases shown correspond to forward scattering of the electron. Cases of very non-relativistic final kinetic energy are not plotted to reduce clutter.

We would like to evaluate the power scaling characteristics for various τ and w_0, extending our region of study to include laser peak powers as low as 5 TW. The results of optimization over ψ_0 - $z(0)$ space are shown in Fig. 4.3.3. To improve readability, we

have normalized the electron's maximum energy gain at each P by the gain limit $\Delta E_{\lim}$ (Eq. (10)), and the electron's optimal initial position by the Rayleigh range z_0. Note that the $w_0 = 2$ μm plots in Fig. 4.3.3(a) are just normalized versions of the dashed lines in Fig. 4.3.1(a). From Fig. 4.3.3, we observe the following trends:

a) Given τ and w_0, a threshold power P_{th} exists such that negligible energy gain is obtained for $P < P_{th}$. P_{th} is approximately independent of τ and is approximated by the condition used in [28] to find the threshold w_0 for given P with $z(0) = 0$:

$$a_0 \equiv \frac{e}{mc\omega z_0}\sqrt{\frac{8\eta_0 P_{th}}{\pi}} \approx 1 \qquad (4.2.11)$$

where a_0 is simply the normalized field amplitude of E_z at the focus. As discussed in [28], Eq. (4.2.11) is motivated by the observation made in ponderomotive acceleration studies (e.g. [17]) that $a_0 \geq 1$ is required to access the relativistic regime of laser-electron interaction (except that for ponderomotive acceleration, a_0 is computed with the transverse rather than longitudinal field amplitude). For $w_0 = 2$, 4, 6, 8, 10, 12 μm, Eq. (4.2.11) gives $P_{th} \approx 4.163\times 10^{-3}$, 6.661×10^{-2}, 3.372×10^{-1}, 1.066, 2.602, 5.396 PW (4 sig. fig.) respectively, which by Fig. 4.3.3(a) are estimates accurate to well within an order of magnitude.

b) Given τ and w_0, energy gain (whether in MeV or normalized by $\Delta E_{\lim}$) increases with increasing P. That the normalized gain asymptotically approaches a constant value tells us that at $P >> P_{th}$, the energy gain in MeV is approximately

proportional to $\sqrt{P}$, a behavior that has been noted for the $z(0) = 0$ case studied in [28].

c) Given w_0 and P, energy gain increases with increasing τ up to an optimal τ and decreases as τ increases further. As the given P decreases toward P_{th}, this optimal τ increases, showing that longer pulses are favored at lower powers. A close-up of Fig. 4.3.3(a) with energy gain in MeV is shown in Fig. 4.3.4 to illustrate this. The conclusion of [28] that a shorter pulse leads to greater net acceleration is thus not generally true.

d) Given τ and P, energy gain decreases with increasing w_0. As far as we can determine in the paraxial wave approximation, the optimal focusing for direct electron acceleration is the tightest.

e) Given τ and w_0, the optimal initial position becomes more negative with increasing P for the vast majority of cases, especially where $P >> P_{th}$, in Fig. 4.3.3(b). At $P \approx P_{th}$, the optimal initial position is close to the focus and may even be slightly positive. For $P >> P_{th}$, the optimal initial position is negative and approximately proportional to $\sqrt[4]{P}$, as we have ascertained by curve-fitting.

f) Given w_0 and P, the optimal initial position becomes more negative with increasing τ for the vast majority of cases, especially where $P >> P_{th}$, in Fig. 4.3.3(b).

g) Given τ and P, the optimal initial position normalized by z_0 becomes more negative with decreasing w_0.

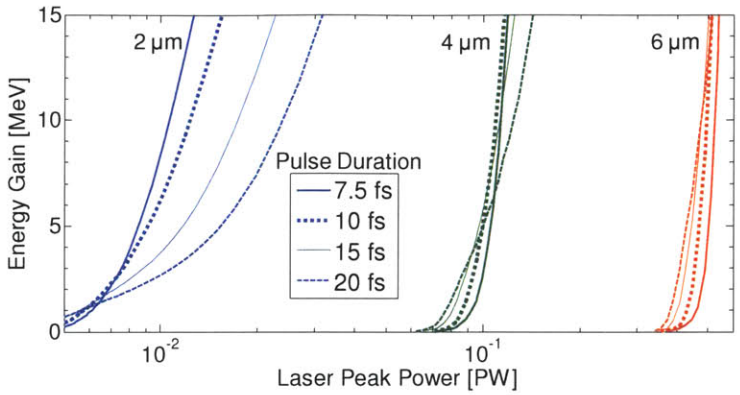

Fig. 4.3.4. Close-up of plot of maximum energy gain vs. P for various w_0 and τ.

One may intuitively expect $z(0) = 0$ to be the optimal initial position in general since, after all, the theoretical gain limit ΔE_{lim} was computed in Eq. (4.2.10) by assuming an electron that enters an accelerating cycle at the laser focus and staying in that cycle forever. However, an electron that starts at rest is bound to slip through a succession of accelerating and decelerating cycles before entering what is effectively its final accelerating cycle (that is, the final accelerating cycle that has any significant impact on its energy) with a velocity that is in general quite different from its initial velocity, so the relationship between $z(0)$ and the electron's final energy gain is complicated. We also note that although including the $z(0)$ dimension in the optimization space significantly increases the electron's energy gain over the $z(0) = 0$ case, the electron still extracts at best less than $\Delta E_{\text{lim}}/2$ of energy from the pulse. In [28], it is argued that sub-cycle direct acceleration can only take place from $z > z_0$ to ∞, so the energy gain will always be less than $\Delta E_{\text{lim}}/2$ for initially stationary electrons. We show in the next section that by using a pre-accelerated electron, we can make the electron enter its final accelerating cycle at a position $z < z_0$ and extract more than $\Delta E_{\text{lim}}/2$ of energy from the pulse

4.4. Direct acceleration of a pre-accelerated electron

For convenience we introduce an artificial parameter D that we call the "protracted collision position" and define as the position where the electron would coincide with the pulse peak if the electron were to always travel at its initial speed $v(0)$:

$$\frac{v(0)}{D - z(0)} \equiv \frac{c}{D - z_i} \Rightarrow D \equiv \frac{z(0) - \beta(0) z_i}{1 - \beta(0)} \tag{4.4.1}$$

For the initially stationary electron studied in the previous section, $\beta(0) = 0$ so $D = z(0)$ as expected. For values of D far enough from the laser focus such that the electron always experiences a negligibly small electric field (resulting in little change in the electron's velocity from its initial value), D approximates the actual position where electron and pulse peak coincide, hence our name for it. In general, however, the position where electron and pulse peak coincide may be very different from D. Although D may not have much physical significance, it is useful as it allows us to control two variables, $z(0)$ and z_i, simultaneously: After specifying D for a particular simulation, we use Eq. (4.4.1) and our knowledge of the electric field profile to determine the set of values $z(0)$ and z_i closest to the focus but such that the effect of the electric field on the electron is initially below an arbitrarily small amount (i.e. the pulse effectively begins infinitely behind the electron, so the electron effectively begins in field-free vacuum). Simply setting z_i to be an arbitrarily large negative number will of course also produce an accurate simulation, but the simulation time will be unnecessarily long.

In Figs. 4.4.1 and 4.4.2, we plot the maximum energy gain (normalized by ΔE_{lim}) and the corresponding optimal D (normalized by z_0) vs. P with w_0 and the electron's initial

kinetic energy $E_K(0)$ as parameters. Fig. 4.4.1 and Fig. 4.4.2 correspond to the case of $\tau = 7.5$ fs and $\tau = 15$ fs respectively. In Fig. 4.4.3, we plot the normalized maximum energy gain vs. $E_K(0)$ with P and w_0 as parameters for $\tau = 10$ fs. The plots in Figs. 4.4.1-2 are obtained by optimizing over ψ_0-D space. From these figures, we observe the following trends:

a) Given τ and w_0, P_{th} decreases with increasing $E_K(0)$. Given τ and $E_K(0)$, P_{th} increases with increasing w_0. P_{th} is approximately independent of τ, as in the $v(0) = 0$ case.

b) Given τ, w_0 and P, there exists an initial kinetic energy threshold E_{Kth} such that negligible energy gain is obtained for $E_K(0) < E_{Kth}$. Given τ and w_0, E_{Kth} decreases with increasing P. Given τ and P, E_{Kth} increases with increasing w_0. E_{Kth} is approximately independent of τ. Although some of these trends are evident from Fig. 4.4.3, they may all be directly inferred from (a), which tells us that P_{th} is a strictly decreasing function of $E_K(0)$ (given τ and w_0 within the parameter space studied). Note also that if P_{th} is a strictly decreasing function of $E_K(0)$, $P = P_{th}$ if and only if $E_K(0) = E_{Kth}$.

c) Given τ, w_0 and P, energy gain increases with increasing $E_K(0)$ at least up to a certain $E_K(0)$. As can be seen from the $w_0 = 2$ μm plot in Fig. 4.4.3(a), the energy gain starts to fall after a certain $E_K(0)$.

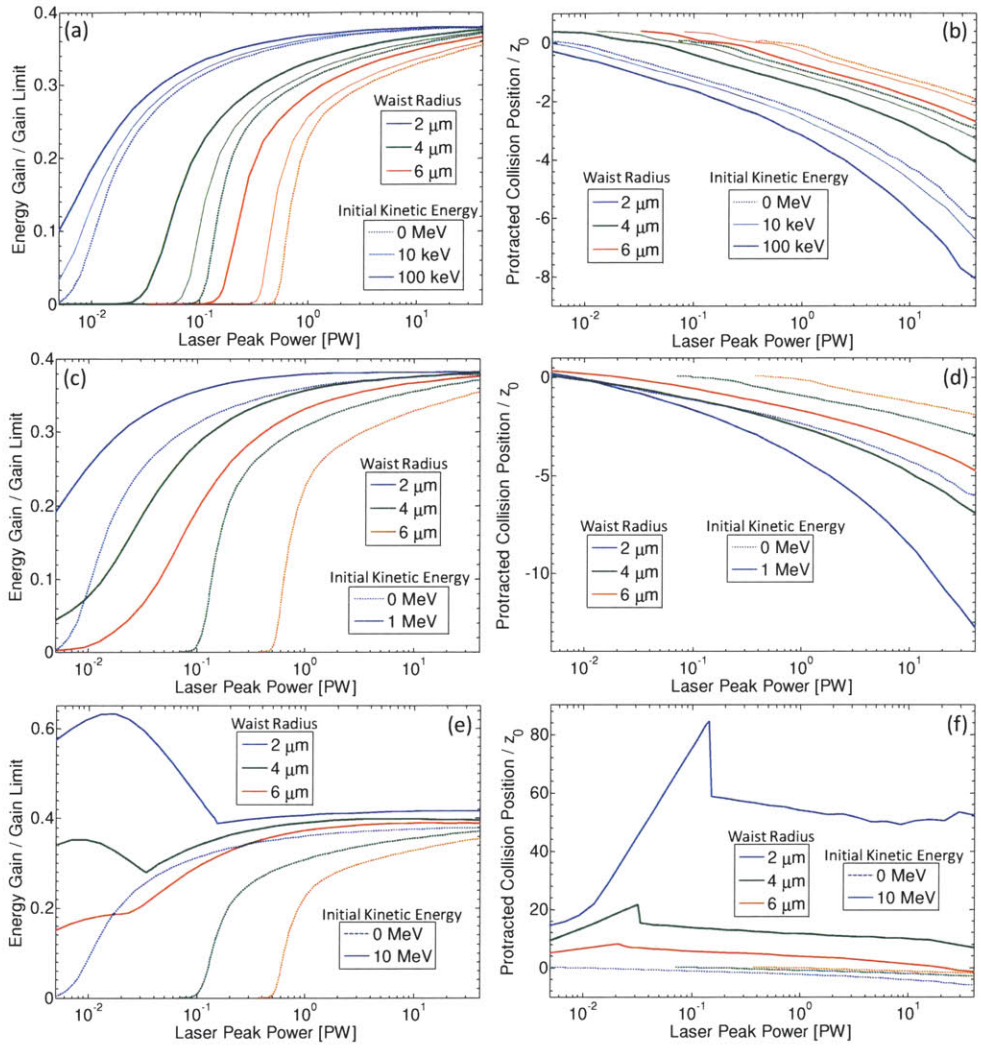

Fig. 4.4.1. Normalized maximum energy gain and corresponding normalized optimal D vs. P from 5 TW to 40 PW for various w_0 and $E_K(0)$: (a), (b) non-relativistic $E_K(0)$; (c), (d) marginally-relativistic $E_K(0)$; and (e), (f) relativistic $E_K(0)$. $\tau = 7.5$ fs. All cases shown correspond to forward scattering of the electron. Cases of very non-relativistic final kinetic energy are not plotted to reduce clutter.

d) Given $E_K(0)$, w_0 and P, energy gain increases with increasing τ up to an optimal τ and decreases as τ increases further. As the given P ($E_K(0)$) decreases toward P_{th} (E_{Kth}), this optimal τ increases, showing that longer pulses are favored at lower powers.

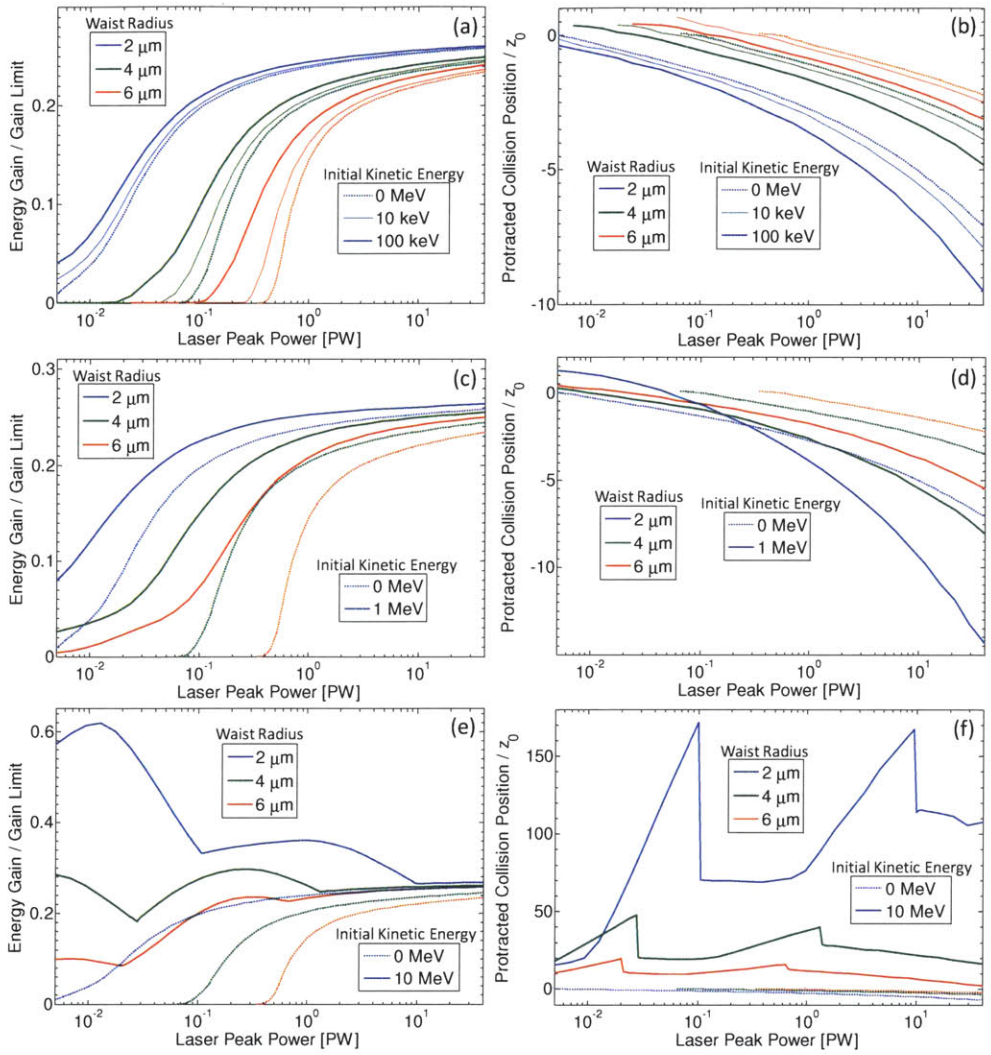

Fig. 4.4.2. Normalized maximum energy gain and corresponding normalized optimal D vs. P from 5 TW to 40 PW for various w_0 and $E_K(0)$: (a), (b) non-relativistic $E_K(0)$; (c), (d) marginally-relativistic $E_K(0)$; and (e), (f) very relativistic $E_K(0)$. $\tau = 15$ fs. All cases shown correspond to forward scattering of the electron. Cases of very non-relativistic final kinetic energy are not plotted to reduce clutter.

e) Given $E_K(0)$, τ and P, energy gain decreases with increasing w_0. Once again, the optimal focusing for direct electron acceleration is the tightest as far as we can determine in the paraxial wave approximation.

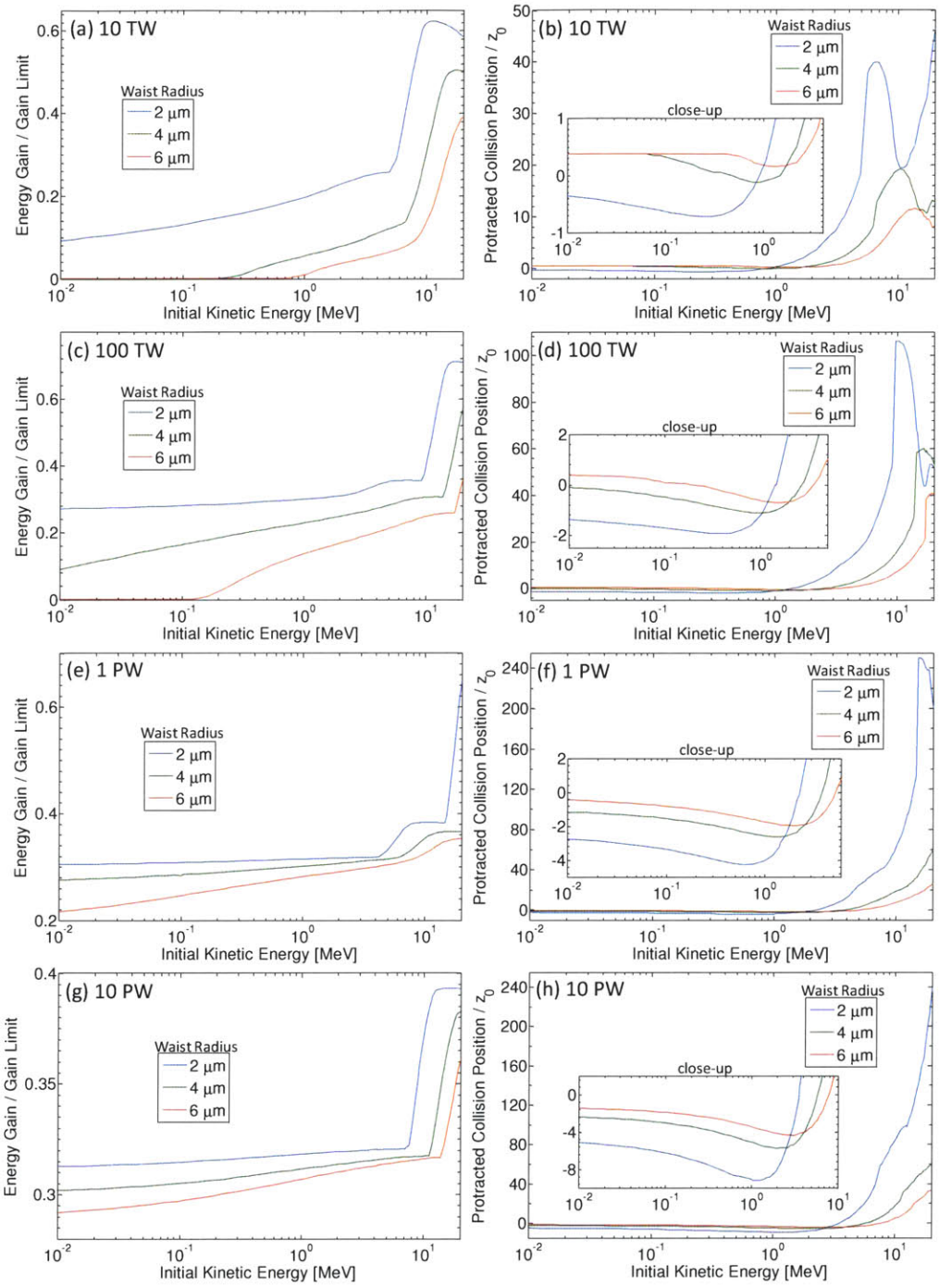

Fig. 4.4.3. Normalized maximum energy gain and corresponding normalized optimal D vs. $E_K(0)$ from 0.01 to 20 MeV for various w_0 and P : (a), (b) P =10 TW; (c), (d) $P = 100$ TW; (e), (f) $P = 1$ PW; and (g), (h) $P = 10$ PW. $\tau = 10$ fs. All cases shown correspond to forward scattering of the electron.

f) Given $E_K(0)$, τ and w_0, the energy gain in MeV increases with increasing P. The energy gain normalized by ΔE_{lim} also increases with increasing P at non-relativistic $E_K(0)$, but this is not true in general at relativistic $E_K(0)$, as is evident from Figs. 4.4.1(e) and 4.4.2(e). Fig 4.4.3 corroborates our conclusion by showing that the normalized energy gain increases with increasing P for values of $E_K(0)$ up to a few MeV, but ceases to always do so beyond this range. Hence, although greater energy gain in MeV can always be achieved (for given $E_K(0)$, τ and w_0) by increasing P and optimizing parameters, the fraction of the theoretical energy gain limit extracted may in fact become smaller if $E_K(0)$ is relativistic.

g) At non-relativistic $E_K(0)$, D decreases from its value for the $v(0)=0$ case with increasing $E_K(0)$. That this decrease is small accords with physical intuition because relative to the speed of the pulse (c), an electron with non-relativistic $E_K(0)$ is practically stationary so one would expect the optimal D to be very close to that for the $v(0)=0$ case. This reasoning, of course, no longer applies at relativistic $E_K(0)$. It is evident from the plots of D in Fig. 4.4.3 that beyond a certain $E_K(0)$ (around 1 MeV) for each plot, the slope of D with respect to $E_K(0)$ is no longer always negative, and D itself may be located up to hundreds of times the Rayleigh range beyond the laser focus.

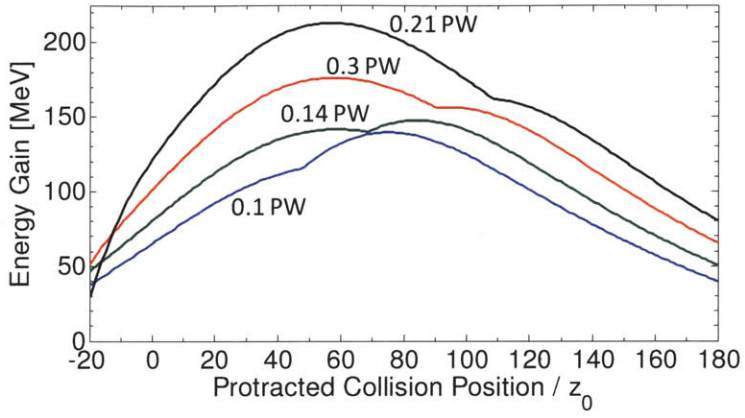

Fig. 4.4.4. Maximum energy gain vs. normalized D for $\tau = 7.5$ fs, $w_0 = 2$ μm and $E_K(0) = 10$ MeV for various P. All cases shown correspond to forward scattering of the electron.

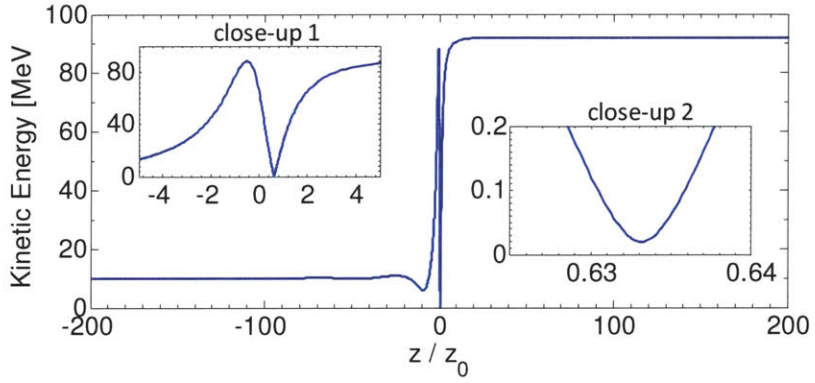

Fig. 4.4.5. Electron kinetic energy vs. normalized position for $P = 17.3$ TW, $w_0 = 2$ μm, $\tau = 7.5$ fs, $E_K(0) = 10$ MeV, and optimal ψ_0 and D. Inset "close-up 2" zooms into the point at which the electron enters its effectively final accelerating cycle.

The discontinuities in Figs. 4.4.1(f) and 4.4.2(f) are due to the existence of multiple energy gain local maxima in D for certain combinations of $E_K(0)$, τ, P and w_0. The cause of the discontinuity around $P = 0.15$ PW for the $w_0 = 2$ μm case of Fig. 4.4.1(f) is illustrated in Fig. 4.4.4, which plots energy gain, maximized over ψ_0 space, as a function of D. Although each local maxima varies continuously as P increases from 0.14 PW to 0.3 PW, the global maximum jumps at some point from one of the local maxima to the

other, resulting in the discontinuity in Fig. 4.4.1(f). Similar situations are responsible for the discontinuities in Fig. 4.4.2(f).

As we have noted, a pre-accelerated electron can gain more than half the theoretical energy gain limit. It does so by entering its effectively final accelerating cycle within a Rayleigh range after passing the laser focus. Fig. 4.4.5 shows a plot of kinetic energy vs. displacement for one of the cases picked from the $w_0 = 2$ μm, $E_K(0) = 10$ MeV curve in Fig. 4.4.1. As we can see, the electron coming in from the left enters its effectively final accelerating cycle with a kinetic energy of a few tens of keV at a displacement of about $z = 0.633\, z_0 < z_0$, and leaves the interaction region with a final kinetic energy of over 90 MeV. The energy gain of over 80 MeV is clearly more than half the theoretical gain limit, which in this case ($P = 17.3$ TW) is about 129 MeV by Eq. (4.2.10).

To give an example of how relatively low-power lasers may be used in a direct acceleration scheme, we see that for either $\tau = 7.5$ fs (Fig. 4.4.1(e)) or $\tau = 15$ fs (Fig. 4.4.2(e)), a pulsed radially-polarized laser beam of $w_0 = 2$ μm and $P = 5$ TW can accelerate an electron from an initial kinetic energy of 10 MeV to a final kinetic energy of about 50 MeV. Eqs. (4.2.4) and (4.2.5) give us pulse energies of about 45 mJ and 90 mJ for the 7.5 fs and 15 fs pulse respectively. This shows that lasers can already be very useful for electron acceleration at relatively low powers, just that the electrons must be pre-accelerated (preferably to relativistic speeds) to extract substantial energy from the laser pulse. Although it appears from our results that a smaller improvement in normalized energy gain is obtained with a pre-accelerated electron at higher laser powers, this does not discount the possibility of substantial improvements at these higher powers if we increase $E_K(0)$ to values beyond the range studied.

As another example, we note from Figs. 4.2.5 and 4.4.3 that a two-stage laser accelerator employing a pulsed radially-polarized laser beam of $w_0 = 2$ μm, $\tau = 10$ fs and $P = 10$ TW (giving a pulse energy of about 120 mJ) in each stage can accelerate an initially stationary electron to a kinetic energy of about 6.3 MeV in the first stage, and thence to a kinetic energy of about 36 MeV in the second stage. Note that the same pulse may be used in both stages, since the pulse transfers a negligible fraction of its energy to the electron in the first stage. Clearly, direct acceleration of electrons to substantial energies in infinite vacuum can in principle be realized without the use of petawatt peak-power laser technology. Lasers with peak powers of a few terawatts are already capable of accelerating electrons to energies of tens of MeV, high enough for applications like the production of hard X-rays via inverse Compton scattering [33]. In addition, recall that we have limited our studies to $w_0 \geq 2$ μm. If energy gain continues to increase with tighter focusing for waist radii below 2 μm, it is likely that much more impressive results (at least in terms of energy gain) may be obtained with lasers focused down to an order of a wavelength.

Because the electron in Fig. 4.4.5 moves at a relativistic speed for most of its trajectory, one may mistakenly expect its energy gain to be approximately 0. This is supported by the egregious approximation that $v(t) \approx c \; \forall t$, which enables an analytic computation of energy gain as (allowing α to be some constant determined by the particle's location relative to the center of the pulse envelope)

$$\Delta E_{v=c} = \int_{-\infty}^{\infty} dz(eE_z) \approx \int_{-\infty}^{\infty} dz\alpha \left[\frac{e/z_0}{1+(z/z_0)^2} \sqrt{\frac{8\eta_0 P}{\pi}} \right] \sin\left(2\tan^{-1}(z/z_0) + \psi_0\right) = 0 \quad (4.4.2)$$

Our exact numerical simulations reveal that this is not the case. Although the electron is relativistic for most of its trajectory, the few places at which it becomes non-relativistic are sufficient to produce an asymmetry that prevents the actual integral of force over distance from vanishing.

This observation also encourages the hypothesis that the highest $E_K(0)$ with which an electron may be substantially accelerated by a pulsed radially-polarized laser beam is on the order of the theoretical gain limit ΔE_{lim}, because ΔE_{lim} also represents the maximum *deceleration* of a pre-accelerated electron. If $E_K(0)$ is relativistic and $E_K(0) >> \Delta E_{\text{lim}}$, the laser field can never at any point decelerate the electron to non-relativistic speeds so $v(t) \approx c \; \forall t$ would be true and Eq. (4.4.2) would hold. This hypothesis may be extended to any other direct acceleration scheme if a corresponding ΔE_{lim} expression may be found for it. The electron's energy gain for a given laser should thus decrease after some point as $E_K(0)$ continues to increase, and become negligible for $E_K(0) >> \Delta E_{\text{lim}}$. This implies that there exists a second set of power and initial kinetic energy threshold values (i.e.: different from the P_{th} and E_{Kth} predicted by (4.2.11)) observable only at values of $E_K(0)$ beyond the range studied given our range of P. This "second threshold" places an upper bound on $E_K(0)$ given P (and continues to place a lower bound on P given $E_K(0)$) for non-negligible acceleration. In the next chapter, we see that our hypothesis is correct and that an analytical formula can be derived to approximate the threshold for net acceleration of an on-axis electron in infinite vacuum by a radially-polarized beam for any initial electron velocity.

5. Linear Acceleration of Relativistic Electrons In Infinite Vacuum Under the Lawson-Woodward Theorem

The Lawson-Woodward theorem (see, for instance, [15]), which has caused some controversy over vacuum electron acceleration schemes [42-47], has often been cited (e.g.: [15,23,24,43]) to discount the possibility of accelerating relativistic particles by direct-field interaction (i.e.: purely by a force linear in the electric field) in infinite vacuum. Simulations [29], however, have shown that an initially-relativistic electron in unbounded space may gain substantial net energy from its interaction with only the on-axis longitudinal component of a pulsed radially-polarized beam (even without taking radiation reaction into account). In this chapter, we derive an analytical expression for the "direct acceleration boundary", the boundary with which the Lawson-Woodward theorem divides the parameter space of direct electron acceleration in infinite vacuum into a region of substantial net energy transfer and a region of negligible net energy transfer. In the process, we shed light on the physics that enables the existence of the former region under the Lawson-Woodward theorem, allowing for the possibility of creating laser-driven particle accelerators that function primarily by linear accelerating forces without requiring components to terminate the laser field close to the beam focus.

The Lawson-Woodward theorem states that under certain restrictive conditions, no net electron energy gain is possible using laser fields. These conditions are [15]

1) The region of interaction is infinite,

2) The laser field is in vacuum with no walls or boundaries present,

3) The electron is highly relativistic along the acceleration path

4) No static electric or magnetic fields are present, and

5) Nonlinear effects like ponderomotive forces and radiation reaction forces are neglected.

The simulations with initially-relativistic particles in Chapter 4 clearly satisfy every one of these five conditions except for condition (3). If condition (3), too, were satisfied, we see from (4.4.2) that we indeed have zero net acceleration, in perfect accordance with the Lawson-Woodward theorem. Fig. 4.4.5, however, tells us that a relativistic particle that experiencing an acceleration linear in the electric field does not necessarily remain relativistic throughout its entire trajectory. This breaks the symmetry that causes (4.4.2) to integrate to 0, allowing for net acceleration.

One would thus postulate that net electron acceleration (neglecting radiation reaction) in a direct acceleration scheme is contingent upon the electron undergoing at least one "quarter-cycle relativistic transition", by which we mean a change from a non-relativistic speed to a relativistic speed or vice versa within one quarter of a cycle, in the course of its interaction with the laser pulse. For an initially-relativistic particle to undergo net acceleration, it would then have to decelerate at least once to non-relativistic speeds before being re-accelerated up to a speed even more relativistic than what it started out with. This is exactly what happens in Fig. 4.4.5, where the 10 MeV electron is accelerated to a final energy of over 90 MeV.

We verify our postulate by using it to derive an equation for the boundary dividing the parameter space of direct electron acceleration by a radially-polarized beam into a region of substantial net acceleration and a region of insubstantial net acceleration. We then verify this predicted boundary is correct by super-imposing it over the results of exact numerical simulations.

In the frame of reference of the on-axis electron at initial time, we have the equation

$$\frac{d(\gamma'\beta')}{dt'} = -\frac{e}{mc} E_z(x=0, y=0, z, t) \tag{5.1}$$

where $E_z(x, y, z, t)$ is the longitudinal component of the electric field in the laboratory frame, and x, y, z, t are the coordinates of that frame. (5.1) holds for any electromagnetic field that completely vanishes on axis except for its E_z component . Throughout this section, we use primes to indicate variables in the electron's frame. Thus, the Lorentz transform gives us the relations $z = \gamma_0(z' + v_0 t')$ and $t = \gamma_0(t' + (v_0/c^2)z')$, where $v_0 = \beta_0 c$ is the initial speed of the electron in the +z direction and $\gamma_0 \equiv 1/\sqrt{1-\beta_0^2}$, in the laboratory frame. Since we argue that a relativistic transition is necessary to give net acceleration and we are interested in computing the threshold at which net acceleration occurs, we may assume that the electron at this boundary is approximately unperturbed by the laser field and set $z' = 0$, giving $z = \gamma_0 v_0 t$ and $t = \gamma_0 t$. Substituting into (5.1), we find

$$\frac{d(\gamma'\beta')}{dt'} \approx -\frac{e}{mc}\sqrt{\frac{8\eta_0 P}{\pi}} \frac{1/z_0}{1+(z/z_0)^2} \sin\left(\omega\gamma_0(1-\beta_0)t' + 2\tan^{-1}\left(\frac{z}{z_0}\right) + \psi_0\right) \tag{5.2}$$

where we have neglected the pulse envelope for simplicity (we will see, in fact that the direct acceleration boundary is independent of pulse duration). Now let $z = z_a$ be the location along the beam axis where the particle is most likely to make a relativistic transition. This would correspond to the location where the amplitude of the $\gamma'\beta'$ oscillation in (5.2) is largest. We Taylor-expand (5.2) about $z = z_a$ to find

$$\frac{d(\gamma'\beta')}{dt'} \approx -\frac{e}{mc}\sqrt{\frac{8\eta_0 P}{\pi}} \frac{1/z_0}{1+(z_a/z_0)^2} \sin\left(\left[\omega\gamma_0(1-\beta_0) + \frac{2\gamma_0 v_0/z_0}{1+(z_a/z_0)^2}\right]t' + \text{constant}\right) \tag{5.3}$$

The oscillation amplitude of $\gamma'\beta'$ is thus given by

$$\gamma'\beta' \sim \frac{e}{mc}\sqrt{\frac{8\eta_0 P}{\pi}}\frac{1/z_0}{1+(z_a/z_0)^2}\left[\omega\gamma_0(1-\beta_0)+\frac{2\gamma_0 v_0/z_0}{1+(z_a/z_0)^2}\right]^{-1} \tag{5.4}$$

By inspection, one sees that the oscillation amplitude is maximized at $z_a = 0$. Making this substitution in (5.4) and setting the expression to 1 (because we can take $\gamma\beta > 1$ as the definition of a relativistic particle and setting (5.4) to 1 would then correspond to the smallest change in momentum that constitutes a relativistic transition in one quarter-cycle of the laser field), we find ourselves with an expression for the threshold power P_{th} as a function of the electron's initial speed

$$P_{th} = \frac{\pi}{8\eta_0}\left(\frac{2mc^2}{e\varepsilon_d^2}\right)^2 \gamma_0^2\left[1-\beta_0\left(1-\varepsilon_d^2\right)\right]^2 \tag{5.5}$$

where $\varepsilon_d \equiv \lambda/\pi w_0$. Note that P_{th} is dependent only on focusing, which is measured by ε_d, and the initial speed of the electron. $P > P_{th}$ must hold for substantial net acceleration.

We now examine (5.5) in the limit $\beta_0 \to 0, \gamma_0 \to 1$, which corresponds to an initially stationary or highly non-relativistic electron. Under these conditions (5.5) gives

$$P_{th} = \frac{\pi}{8\eta_0}\left(\frac{2mc^2}{e\varepsilon_d^2}\right)^2 \tag{5.6}$$

which is simply the acceleration threshold for an initially stationary electron [28, 29]. In the limit of an initially highly-relativistic electron, $\beta_0 \to 1, \gamma_0 >> 1$ and (5.5) becomes

$$P_{th} = \frac{\pi}{8\eta_0}\left(\frac{2mc^2}{e}\right)^2 \gamma_0^2 \tag{5.7}$$

This may simply be recast as $e\sqrt{8\eta_0 P_{th}/\pi}/2 = \gamma_0 mc^2 = 0.5\Delta E_{\lim}$, where $\Delta E_{\lim}$ is the theoretical gain limit [28, 29] under highly idealized conditions and imposes a ceiling on the amount of net energy an on-axis electron can possibly gain in a single pass through a radially-polarized laser beam. (5.7) thus tells us that for an initially highly-relativistic electron to gain substantial net energy via direct acceleration by a radially-polarized beam, the initial energy of the electron must be less than a value on the order of the theoretical gain limit, which makes intuitive sense. (5.7) also confirms the hypothesis made in Chapter 4 and in [29] that substantial electron acceleration cannot be achieved if the electron's initial kinetic energy greatly exceeds the laser's theoretical gain limit. Hence, net acceleration of relativistic electrons by direct acceleration in infinite vacuum is possible as long as the laser's peak pulse power is high enough relative to the energy of the electron.

To verify the accuracy of (5.5), we compute the maximum energy gain in P-γ_0 space, optimizing over ψ_0-$z(0)$ space at every point, for a given τ and w_0. Our results are shown in Fig. 5.1 for various values of w_0.

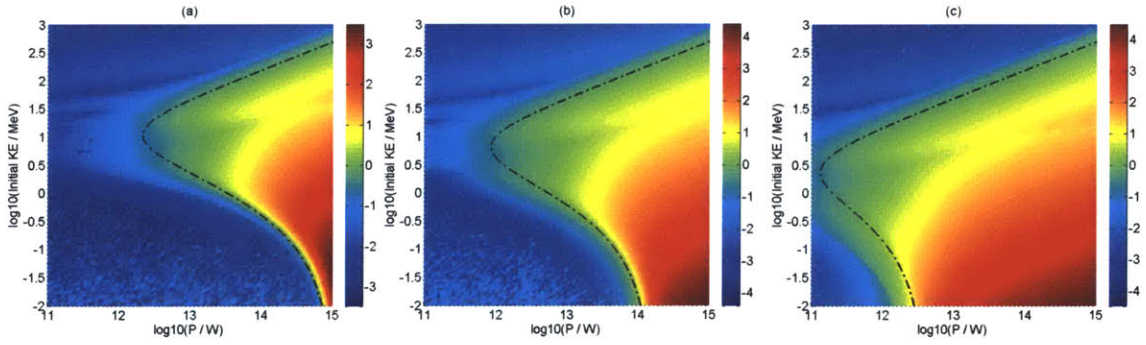

Fig. 5.1. Surface plots of log10(Net Energy Gain / Initial KE) for a) $w_0 = 8\mu m$, b) $w_0 = 5\mu m$ and c) $w_0 = 2\mu m$. $\lambda = 0.8\mu m$ and $\tau = 10fs$. Each point has been optimized for energy gain over ψ_0-$z(0)$ space. "KE" stands for kinetic energy. Dash-dotted lines mark the direct acceleration boundary described by (5.5).

From Fig. 5.1, we see that (5.5) provides a very good approximation of the boundary between substantial and negligible net acceleration in the parameter space. For every value of initial electron energy, there exists a threshold peak laser power below which negligible net acceleration is obtained. For every value of peak laser power, there exists a finite range of initial electron energies within which substantial acceleration can occur. At lower initial peak powers, there is both an upper and lower bound on the initial electron energies. At higher initial peak powers, the lower bound disappears, allowing for the acceleration of rest electrons to relativistic energies. With increased focusing, the direct acceleration boundary expands to include more of the P - γ_0 parameter space. Note that the boundary at higher values of γ_0 does not change much with focusing. This is predicted by (5.7), which is independent of ε_d (unlike (5.6)).

We may also simulate over P - w_0 space for a given value of γ_0 to obtain Fig. 5.2.

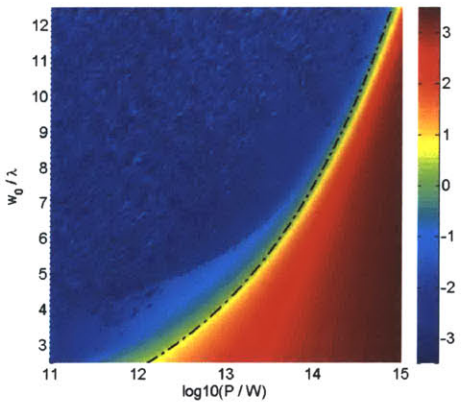

Fig. 5.2. Surface plot of log10(Net Energy Gain / Initial KE). $\tau = 10\text{fs}$. Initial KE is 100 keV. Each point has been optimized for energy gain over ψ_0 - $z(0)$ space. "KE" stands for kinetic energy. Dash-dotted line marks the direct acceleration boundary described by (5.5).

Fig. 5.2 verifies (5.5) and shows that for substantial acceleration, a low peak power laser requires a tighter focusing. This makes sense since being able to achieve a quarter-

cycle relativistic transition, which we have argued is necessary for substantial acceleration, requires a certain minimum intensity at the laser focus.

To show that the direct acceleration boundary is relatively independent of pulse duration, we may sweep over τ - P space to obtain Fig. 5.3.

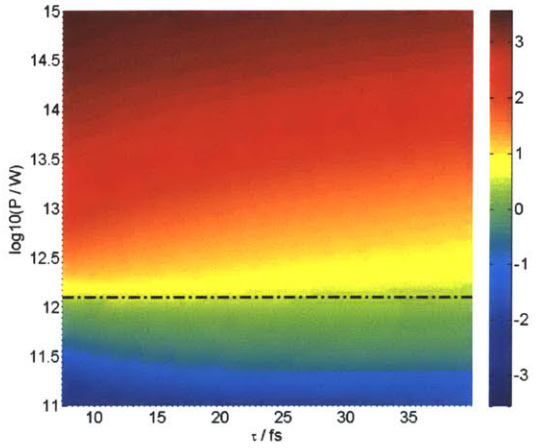

Fig. 5.3. Surface plot of log10(Net Energy Gain / Initial KE). $\lambda = 0.8\mu m$ and $w_0 = 2\mu m$. Initial KE is 100 keV. Each point has been optimized for energy gain over ψ_0 - $z(0)$ space. "KE" stands for kinetic energy. Dash-dotted line marks the direct acceleration boundary described by (5.5).

Fig. 5.3 shows that the acceleration threshold is relatively independent of pulse duration, although one can see that the energy gain at higher powers is better with smaller pulse durations, while the non-relativistic energy gains at powers below the threshold seem to be optimized at larger pulse durations (this agrees with observations made in [29]).

We therefore see that the Lawson-Woodward theorem does not preclude substantial net acceleration of an electron through linear interaction with an electromagnetic field in unbounded space. There exists a subset of parameters in the parameter space where one of the conditions of the theorem, namely that the electron remains highly-relativistic

throughout its trajectory, can be broken by the electron undergoing a quarter-cycle relativistic transition in the course of its interaction with the laser pulse, allowing for net energy gain. For a radially-polarized laser beam, the boundary for direct on-axis electron acceleration is given by (5.5). Our calculations, however, may be generalized to any scheme in which an electron is linearly accelerated by a propagating electromagnetic wave's longitudinal electric field component (with all other electromagnetic components absent). Repeating our procedure for a general electrodynamic equation of the form

$$\frac{d(\gamma'\beta')}{dt'} = A(z)\sin(\omega t - kz + B(z)) \tag{5.8}$$

one finds that the direct acceleration boundary is simply approximated by the formula

$$M\left(\frac{|A(z)|}{\omega\gamma_0(1-\beta_0)+dB(z)/dz}, z\right) = 1 \tag{5.9}$$

where the operation $M(f(z), z)$ involves maximizing the function $f(z)$ over z.

6. Two-Color Laser-Driven Direct Acceleration of an Electron in Infinite Vacuum

In this chapter, we show that a two-color pulsed beam can accelerate an electron by over 90% of the one-color beam's theoretical gain limit, for a given total energy and pulse duration. The scheme exploits how the Gouy phase shift will vary the interference pattern of the on-axis electric field with position along the beam axis. For most cases well above the threshold power for electron acceleration, maximum acceleration is obtained with an acceleration-favoring interference of fields only as the electron enters its effectively final accelerating cycle.

The two-color pulsed beam is the sum of two co-propagating pulsed radially-polarized laser beams, with central angular frequencies ω and 2ω, of equal pulse duration, peak power and Rayleigh range. The electron begins at rest on the beam axis in field-free vacuum (the pulse begins infinitely far away) and ends moving in field-free vacuum after the pulse has completely overtaken it (the setup is identical to that in Chapter 4, with the one-color beam replaced by a two-color beam). On the beam axis all transverse fields vanish, leaving the longitudinal electric field E_z, which is obtained by summing the E_z components of two one-color beams:

$$E_z = \left[\frac{1/z_0}{1+(z/z_0)^2}\sqrt{\frac{4\eta_0 P}{\pi}}\right]\left[\sin\left((\xi+\psi_a)+\psi_g+\psi_b\right)+\sin\left(2(\xi+\psi_a)+\psi_g+\psi_b\right)\right]\operatorname{sech}\left(\frac{\xi+kz_i}{\xi_0}\right) \tag{6.1}$$

where $\xi \equiv \omega t - kz$; $z_0 \equiv \pi w_0^{\,2}/\lambda$ is the Rayleigh range; $k \equiv 2\pi/\lambda = \omega/c$; w_0 is the waist radius of the fundamental harmonic beam; $\psi_g \equiv 2\tan^{-1}(z/z_0)$ is the Gouy phase shift; $\eta_0 \cong 120\pi\,\Omega$ is the vacuum wave impedance; z_i is the pulse's initial position (effectively $-\infty$); c is the speed of light in vacuum; $\xi_0 \equiv \omega\tau/\mathrm{sech}^{-1}(\exp(-1))$, where τ is the pulse duration; ψ_a and ψ_b are phase constants; $P/2$ is the peak power of each pulse; $z(0)$ is the initial electron position.

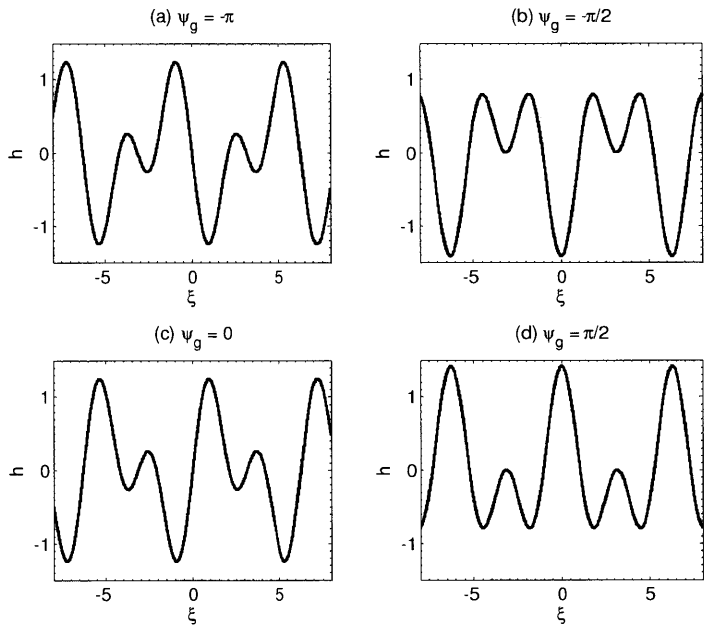

Fig. 6.1. Plots of $h \equiv \sqrt{0.5}\left[\sin(\xi+\psi_g)+\sin(2\xi+\psi_g)\right]$ for various ψ_g.

Our results should closely approximate those for the more general case of a slightly off-axis, non-relativistic electron, due to the electron confinement property of the transverse fields [26,27] and the fact that the laser pulse and phase move at or beyond the speed of light.

Consider the function $h \equiv \sqrt{0.5}\left[\sin\left(\xi + \psi_g\right) + \sin\left(2\xi + \psi_g\right)\right]$, to which Eq. (6.1) is proportional except for a translation in ξ and ψ_g, plotted in Fig 6.1. The phase ψ_b in Eq. (6.1) controls the field pattern produced by interference at each position along the beam axis. For instance, setting $\psi_b = \pi$ would cause the field pattern to evolve, due to the Gouy phase shift, in the order (c)-(d)-(a)-(b)-(c) as the laser pulse propagates from $z = -\infty$ to $-z_0$, 0, z_0 and ∞ respectively. We also note that of all possible patterns, the one in Fig 6.1(b) seems to favor electron acceleration most, since its ratio of most negative to most positive value is largest in magnitude. The position where the Fig 6.1(b) wave pattern occurs is given by $z_b = -z_0 \tan\left(\pi/4 + \psi_b/2\right)$.

We numerically solve the Newton-Lorentz equations of motion using the Adams-Bashforth-Moulton method (*ode113* of *Matlab*). Although we set $\lambda = 0.8$ μm here, our results are readily scalable to any λ since the electrodynamic equations are independent of λ under the normalizations $\mathrm{T} \equiv \omega t$, $\varsigma \equiv z / z_0$ (with $\varsigma_i \equiv z_i / z_0$) and $\kappa \equiv k z_0 = 2\left(\pi w_0 / \lambda\right)^2$ (as was explicitly shown for the one-color beam in Chapter 4). We sweep over P - τ - w_0 space and optimize over ψ_a - ψ_b - $z(0)$ space for electron energy gain normalized by the one-color theoretical energy gain limit ΔE_{lim} given by (4.2.10). As Fig 6.2(a) shows, the two-color beam with peak power $P/2$ in each beam, and therefore the same total power as the one-color beam ($\lambda = 0.8$) with peak power P, can accelerate an electron by more than 90% of the one-color beam's theoretical gain limit, whereas the one-color beam can manage less than 40% in the parameter space studied.

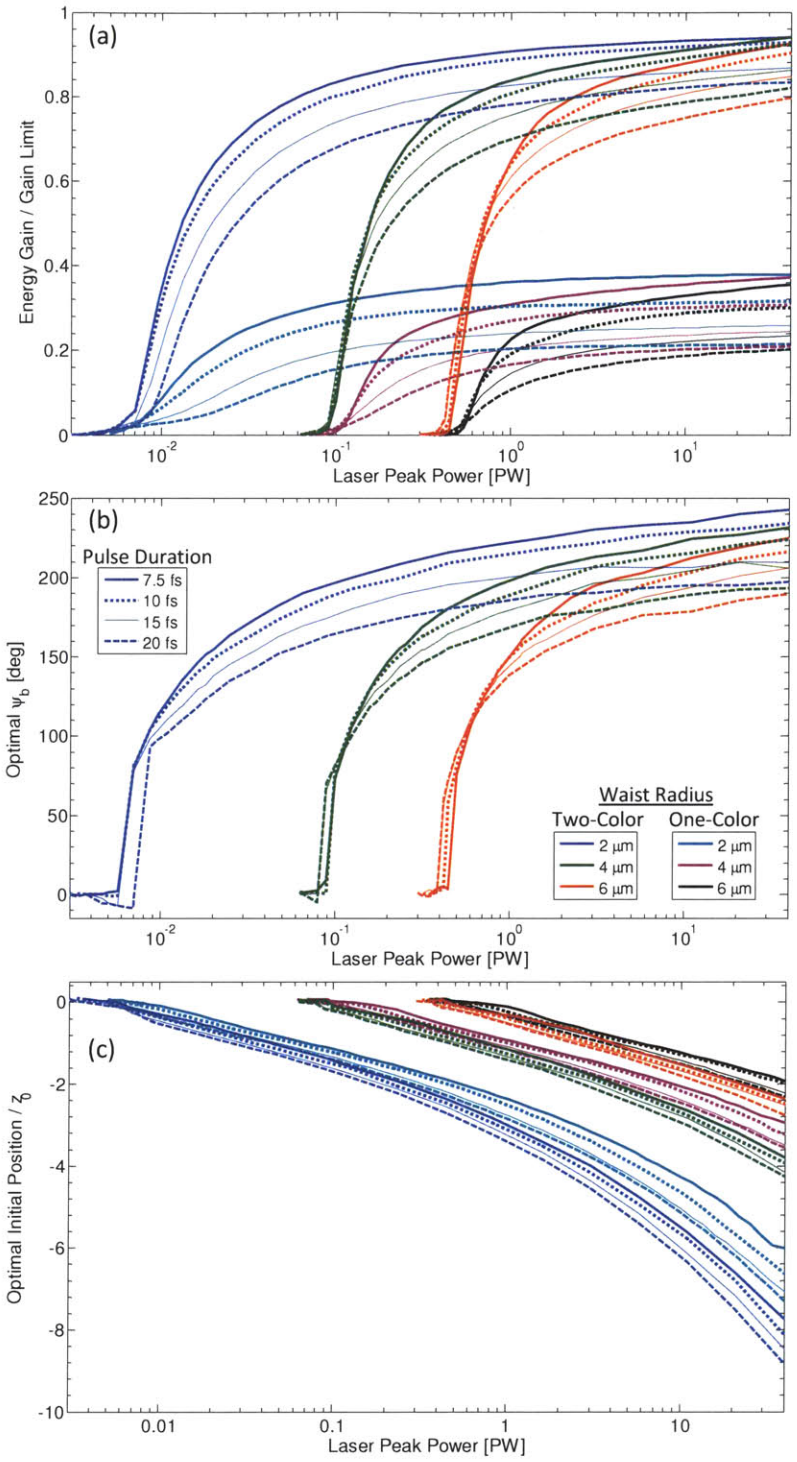

Fig. 6.2. Plots of (a) maximum normalized energy gain (b) corresponding optimal ψ_b (for two-color case) and (c) corresponding optimal normalized $z(0)$ vs. peak power.

Fig 6.2(b) shows that well above the threshold power, the optimal ψ_b lies between $\pi/2$ and $3\pi/2$, i.e. the Fig 6.1(b) wave pattern occurs between $z=0$ and $z=\infty$, with a

tendency to be around π (the Fig 6.1(b) wave pattern occurs around $z = z_0$). This accords with physical intuition because a) due to the Gouy phase shift the electron can enter its effectively final accelerating cycle only after $z = 0$ and b) when determining the best position for the Fig 6.1(b) pattern, one must strike a compromise between the Lorentzian decay (due to beam divergence) in Eq. (6.1) and the fact that the acceleration-favoring Fig 6.1(b) pattern will be maintained over a greater distance the further from the focus it occurs, due to the smaller rate of change with distance of the Gouy phase shift. Fig 6.2(c) shows that the optimal initial position of the initially-stationary electron for the two-color beam tends to be slightly more negative than that for the one-color beam with the same peak power P, pulse duration τ and waist radius w_0.

We have omitted plots of optimal ψ_a vs. P because they consist of points erratically scattered between 0 and 2π radians, with no discernible pattern as a function of P. This apparently erratic behavior arises from the fact that the optimal ψ_a varies rapidly over a small interval in P, and this rapidly-varying pattern can be captured only with simulations of a very high density that are too expensive in terms of simulation time for the method we use here. In practice, one will have to seek the optimal ψ_a manually during an experiment or run a simulation specially for that case, given all other optimal conditions from our analysis.

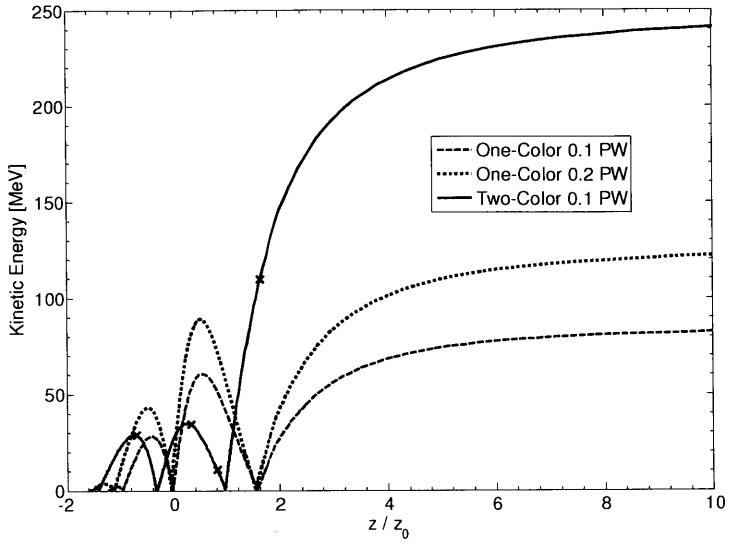

Fig. 6.3. Variation of kinetic energy with electron displacement of an electron hit by a pulse. In each case, $w_0 = 2\ \mu\text{m}$ and $\tau = 10$ fs, with all other parameters optimized. Crosses on the solid curve indicate the positions where the Fig. 6.4 plots are generated.

Applying the same method by which ΔE_{lim} was formulated for the one-color beam gives us a theoretical gain limit for the two-color beam: $\Delta E_{\text{lim},TC} = 2^{1/2} \Delta E_{\text{lim}}$ (given P). This may lead one to expect a two-color beam of total power P and a one-color beam of power $2P$ to be comparable in electron acceleration capability. However, the former in fact significantly outperforms the latter for P well above the electron acceleration threshold. As Fig 6.3 shows, an electron in a 0.1 PW one-color beam slips through several accelerating and decelerating cycles, gaining and losing substantial amounts of energy, before finally entering its effectively final accelerating cycle. When the one-color beam is intensified to 0.2 PW (and optimum conditions re-computed), the final electron energy increases, but so have the heights of the intermediate energy peaks, which reduce net acceleration in this case by pushing back the position where the electron enters its final accelerating cycle. The two-color beam scheme achieves smaller

intermediate peaks by varying the laser's interference pattern to increasingly favor acceleration as the electron moves forward past the focus (Fig 6.4), adopting the acceleration-favoring Fig 6.1(b) pattern only as the electron enters its effectively final accelerating cycle, instead of maintaining the same peak accelerating field at every position as the one-color beam does.

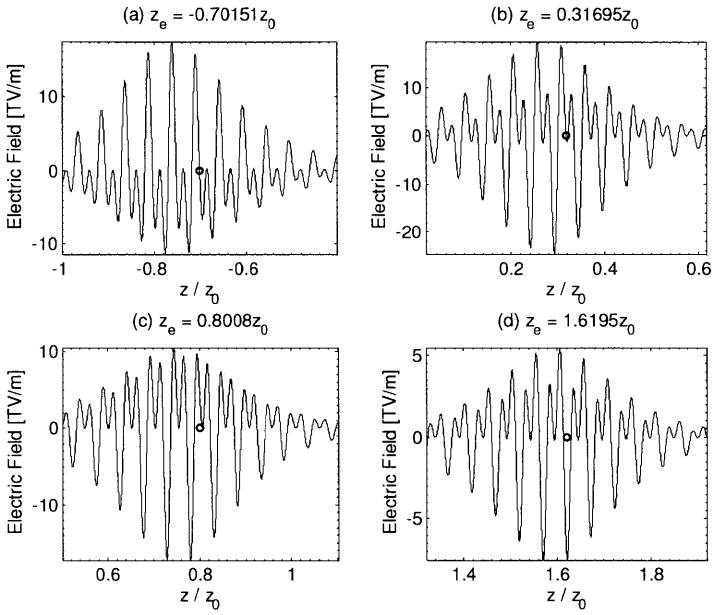

Fig. 6.4. E_z profile of laser pulse at selected positions of the electron's trajectory for the two-color $P = 0.1$ PW case in Fig. 6.3. Circles at $z = z_e$ indicate the electron's position. (a), (b), (c) and (d) correspond respectively to the crosses in Fig. 6.3 from left to right.

Note that our scheme is fundamentally different from vacuum beat wave acceleration [14,15], which also uses a superposition of co-propagating laser beams, but which accelerates electrons by the beat wave arising from the $-e\vec{v}\times\vec{B}$ (ponderomotive force) term in the Lorentz force equation $\vec{F} = -e\left(\vec{E} + \vec{v}\times\vec{B}\right)$, whereas our scheme accelerates electrons by the $-e\vec{E}$ term, using the Gouy phase shift to vary the overall interference pattern with position along the axis.

7. Conclusion

In this thesis, I have reviewed the theory of laser wakefield acceleration and self-focusing of the driver beam in the plasma. In particular, I have shown that the theory of [36] also predicts the existence of higher-order plasma modes, an observation which was not made in [36]. I have studied ponderomotive acceleration in infinite vacuum and shown that the transverse scattering angle of the accelerated electron may be kept small with a proper choice of parameters. I have analyzed the direct acceleration of an electron in infinite vacuum by a pulsed radially-polarized laser beam, consequently demonstrating the possibility of accelerating an initially-relativistic electron in vacuum without the use of ponderomotive forces or any optical devices to terminate the laser field. I have also reconciled the phenomenon of direct acceleration of a relativistic electron in infinite vacuum with the well-known Lawson-Woodward theorem by showing how the space of laser and electron parameters contains a regime where the Lawson-Woodward theorem allows the electron to gain net energy. I also derive an analytical formula for the boundary of this regime. Finally, I have proposed and analyzed a direct electron acceleration scheme that uses a superposition of two pulsed radially-polarized laser beams an octave apart in carrier frequency. This two-color scheme exploits the Gouy phase shift to achieve electron acceleration exceeding 90% of the one-color theoretical energy gain limit, over twice of what is possible with a one-color pulsed beam of equal total energy and pulse duration.

Because direct acceleration of electrons in infinite vacuum by a radially-polarized laser beam benefits from the low radiative losses of direct acceleration, the absence of limits on laser field intensity and electron confinement to the vicinity of the beam axis,

this scheme is a promising candidate for the efficient production of x-rays via inverse Compton Scattering. Future work includes studies on electron beam emittance and energy spread in the vacuum-based schemes explored in this thesis, optimization of accelerated electron bunches for inverse Compton Scattering and the effect of radiation reaction on electron beams accelerated by the linear and ponderomotive forces of laser pulses in infinite vacuum.

Bibliography

1. V. Malka, J. Faure, Y. A. Gauduel, E. Lefebvre, A. Rousse, and K. T. Phuoc, "Principles and applications of compact laser–plasma accelerators," Nat. Phys. **4**(6), 447–453 (2008).
2. J. Badziak, "Laser-driven generation of fast particles," Opto-Electron. Rev. **15**, 1-12 (2007).
3. D. Strickland, and G. Mourou, "Compression of amplified chirped optical pulses," Opt. Commun. **56**(3), 219–221 (1985).
4. M. D. Perry, D. Pennington, B. C. Stuart, G. Tietbohl, J. A. Britten, C. Brown, S. Herman, B. Golick, M. Kartz, J. Miller, H. T. Powell, M. Vergino, and V. Yanovsky, "Petawatt laser pulses," Opt. Lett. **24**(3), 160–162 (1999).
5. S. V. Bulanov, T. Esirkepov, and T. Tajima, "Light intensification towards the Schwinger limit," Phys. Rev. Lett. **91**(8), 085001 (2003).
6. E. Esarey, C. B. Schroeder, and W. P. Leemans, "Physics of laser-driven plasma-based electron accelerators," Rev. Mod. Phys. **81**(3), 1229–1285 (2009).
7. Y. I. Salamin, S. X. Hu, K. Z. Hatsagortsyan, and C. H. Keitel, "Relativistic high-power laser-matter interactions," Phys. Rep. **427**(2-3), 41–155 (2006).
8. A. Modena, Z. Najmudin, A. E. Dangor, C. E. Clayton, K. A. Marsh, C.Joshi, V.Malka, C. B. Darrow, C.Danson, D. Neely & F. N. Walsh, " Electron acceleration from the breaking of relativistic plasma waves", Nature **377**, 606-608 (1995).
9. C. G. R. Geddes, Cs. Toth, J. van Tilborg, E. Esarey, C. B. Schroeder, D. Bruhwiler, C. Nieter, J. Cary and W. P. Leemans, "High-quality electron beams

from a laser wakefield accelerator using plasma-channel guiding," Nature **431**, 538–541 (2004).

10. S. P. D. Mangles, C. D. Murphy, Z. Najmudin, A. G. R. Thomas, J. L. Collier, A. E. Dangor, E. J. Divall, P. S. Foster, J. G. Gallacher, C. J. Hooker, D. A. Jaroszynski, A. J. Langley, W. B. Mori, P. A. Norreys, F. S. Tsung, R. Viskup, B. R. Walton and K. Krushelnick, "Monoenergetic beams of relativistic electrons from intense laser–plasma interactions," Nature **431**, 535–538 (2004)
11. J. Faure, Y. Glinec, A. Pukhov, S. Kiselev, S. Gordienko, E. Lefebvre, J.-P. Rousseau, F. Burgy and V. Malka, "A laser–plasma accelerator producing monoenergetic electron beams," Nature **431**, 541–544 (2004).
12. E. D. Courant, C. Pellegrini and W. Zakowicz, "High-energy inverse free-electron-laser accelerator," Phys. Rev. A **32**, 2813-2823 (1985).
13. W. D. Kimura, A. van Steenbergen, M. Babzien, I. Ben-Zvi, L. P. Campbell, D. B. Cline, C. E. Dilley, J. C. Gallardo, S. C. Gottschalk, P. He, K. P. Kusche, Y. Liu, R. H. Pantell, I. V. Pogorelsky, D. C. Quimby, J. Skaritka, L. C. Steinhauer and V. Yakimenko, "First Staging of Two Laser Accelerators," Phys. Rev. Lett. **86**, 4041–4043 (2001).
14. H. Hora, "Particle acceleration by superposition of frequency-controlled laser pulses," Nature **333**, 337 (1988).
15. E. Esarey, P. Sprangle, and J. Krall, "Laser acceleration of electrons in vacuum," Phys. Rev. E **52**, 5443 (1995).
16. F. V. Hartemann, S. N. Fochs, G. P. Le Sage, N. C. Luhmann Jr., J. G. Woodworth, M. D. Perry, Y. J. Chen and A. K. Kerman, "Nonlinear

ponderomotive scattering of relativistic electrons by an intense laser field at focus," Phys. Rev. E **51**, 4833 (1995).

17. B. Quesnel and P. Mora, "Theory and simulation of the interaction of ultraintense laser pulses with electrons in vacuum," Phys. Rev. E 58, 3719 (1998).
18. G. Malka, E. Lefebvre, and J. L. Miquel, "Experimental observation of electrons accelerated in vacuum to relativistic energies by a high-intensity laser," Phys. Rev. Lett. 78, 3314 (1997).
19. G. V. Stupakov and M. S. Zolotorev, "Ponderomotive laser acceleration and focusing in vacuum for generation of attosecond electron bunches," Phys. Rev. Lett **86**, 5274-5277 (2001).
20. P. X. Wang, Y. K. Ho, X. Q. Yuan, Q. Kong, N. Cao, A. M. Sessler, E. Esarey and Y. Nishida, "Vacuum electron acceleration by an intense laser," Appl. Phys. Lett. **78**, 2253 (2001).
21. Y. I. Salamin and C. H. Keitel, "Electron acceleration by a tightly focused laser beam," Phys. Rev. Lett. 88, 095005 (2002).
22. S. X. Hu and A. F. Starace, "GeV electrons from ultraintense laser interaction with highly charged ions," Phys. Rev. Lett. **88**, 245003 (2002).
23. T. Plettner, R. L. Byer, E. Colby, B. Cowan, C. M. S. Sears, J. E. Spencer and R. H. Siemann, "Visible-laser acceleration of relativistic electrons in a semi-finite vacuum," Phys. Rev. Lett. 95, 134801 (2005).
24. Y. C. Huang, D. Zheng, W. M. Tulloch and R. L. Byer, "Proposed structure for a crossed-laser beam, GeV per meter gradient, vacuum electron linear accelerator," Appl. Phys. Lett. **68**, 753-755 (1996).

25. M. O. Scully and M. S. Zubairy, "Simple laser accelerator: Optics and particle dynamics," Phys. Rev. A **44**, 2656 (1991).

26. Y. I. Salamin, "Electron acceleration from rest in vacuum by an axicon Gaussian laser beam," Phys. Rev. A **73**, 043402 (2006).

27. Y. I. Salamin, "Mono-energetic GeV electrons from ionization in a radially-polarized laser beam ," Opt. Lett. **32**, 90-92 (2007).

28. P.-L. Fortin, M. Piché, and C. Varin, "Direct-field electron acceleration with ultrafast radially-polarized laser beams: Scaling laws and optimization," J. Phys. B: At. Mol. Opt. Phys. **43** 025401 (2010).

29. L.J. Wong and F. X. Kärtner, "Direct acceleration of an electron in infinite vacuum by a pulsed radially-polarized laser beam," Opt. Express **18**, 25035–25051 (2010).

30. L. J. Wong and F. X. Kärtner, "Two-color-laser-driven direct electron acceleration in infinite vacuum," Opt. Lett. **36**, 957-959 (2011).

31. C. Varin, M. Piché, and M. A. Porras, "Acceleration of electrons from rest to GeV energies by ultrashort transverse magnetic laser pulses in free space," Phys. Rev. E **71**, 026603 (2005).

32. A. Karmakar and A. Pukhov, "Collimated attosecond GeV electron bunches from ionization of high-Z material by radially polarized ultra-relativistic laser pulses," Laser Part. Beams **25**, 371-377 (2007).

33. W. S. Graves, W. Brown, F. X. Kärtner, D. E. Moncton, "MIT inverse Compton source concept," Nucl. Instr. and Meth. A **608**, S103-S105 (2009).

34. P. Sprangle, E. Esarey, J. Krall, and G. Joyce, "Propagation and guiding of intense laser pulses in plasmas," Phys. Rev. Lett. 69, 2200–2203 (1992).

35. A. Pukhov and Meyer-ter-Vehn, J. "Laser wake field acceleration: the highly non-linear broken-wave regime," Appl. Phys. B **74**, 355–361 (2002)

36. G.-Z. Sun, E. Ott, Y. C. Lee and P. Guzdar, "Self-focusing of short intense pulses in plasmas," Phys. Fluids **30**, 526-532 (1986).

37. T. Kurki-Suonio, P. J. Morrison, and T. Tajima, " Self-focusing of an optical beam in a plasma," Phys. Rev. A **40**, 3230–3239 (1989)

38. P. Sprangle, E. Esarey and A. Ting, "Nonlinear interaction of intense laser pulses in plasmas," Phys. Rev. A **41**(8), pp. 4463-69 (1990).

39. C. G. R. Geddes, E. Cormier-Michel, E. Esarey, C. B. Schroeder, P. Mullowney, K. Paul, J. R. Cary, and W. P. Leemans, "Laser-Plasma Wakefield Acceleration with Higher Order Laser Modes," AIP Conf. Proc. 1299, 197 (2010).

40. K. T. MacDonald, "Gaussian laser beams with radial polarization" (2000). http://puhep1.princeton.edu/~mcdonald/examples/axicon.pdf

41. E, Esarey and M. Pilloff, "Trapping and acceleration in nonlinear plasma waves," Phys. Plasmas **2**, 1432-1436 (1995).

42. C. M. Haaland, "Laser electron acceleration in vacuum," Opt. Comm. **114**, 280-284 (1995).

43. P Sprangle, E. Esarey, J. Krall and A. Ting, "Vacuum laser acceleration," Opt. Comm. **124**, 69-73 (1996).

44. C. M. Haaland, "Response to comments on laser electron acceleration in vacuum," Opt. Comm. **124**, 74-78 (1996).

45. A. L. Troha, J. R. Van Meter, E. C. Landahl, R. M. Alvis, Z. A. Unterberg, K. Li, N. C. Luhmann, Jr., A. K. Kerman and F. V. Hartemann, "Vacuum electron acceleration by coherent dipole radiation," Phys. Rev. E **60**(1), 926-934 (1999).

46. J. X. Wang, W. Scheid, M. Hoelss and Y. K. Ho, "Comment on 'Vacuum electron acceleration by coherent dipole radiation'," Phys. Rev. E **65**, 028501 (2002).

47. A. L. Troha and F. V. Hartemann, "Reply to 'Comment on "Vacuum electron acceleration by coherent dipole radiation"'," Phys. Rev. E **65**, 028502 (2002).